Heliyon 9 (2023) e17533

Contents lists available at ScienceDirect

Heliyon

journal homepage: www.cell.com/heliyon

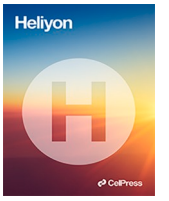

Numerical computation of pulsatile hemodynamics and diagnostic concern of coronary bifurcated artery flow for Newtonian and non-Newtonian fluid

Md. Jashim Uddin [a,b,c], M.Z.I. Bangalee [a,b,*], M. Ferdows [a,b]

[a] Department of Applied Mathematics, University of Dhaka, Dhaka-1000, Bangladesh
[b] Research Group of Fluid Flow Modeling and Simulation, Department of Applied Mathematics, University of Dhaka, Dhaka-1000, Bangladesh
[c] Department of Applied Mathematics, Noakhali Science and Technology University, Noakhali-3814, Bangladesh

ARTICLE INFO

Keywords:
CFD
Pulsatile flow
Pressure drop
Recirculation length
Lesion flow coefficient
Importance factor(IFc)

ABSTRACT

Atherosclerotic with the high occurrence of plaque formation due to stenosis has attracted wide attention among researchers. The left coronary artery has been studied in two-dimensional and in three-dimensional (3D) bifurcation as the models of blood flow through Newtonian and non-Newtonian fluids to better understand the physical mechanism. The computational Fluid Dynamics (CFD) technique is incorporated in COMSOL Multiphysics and then it is justified by satisfactory validation. It is found that the Newtonian model shows larger recirculation zones than non-Newtonian does. The present study also focuses on the evaluations of the lesion of diagnostic and the coefficient of pressure drop assessments on the basis of the diagnostic parameter's critical values affected by the rheological model. Nevertheless, the leading concentration of the subsisting investigation works is confined to the change of importance factor (IFc) affected by arterial blockage. But the IFc of non-Newtonian fluid for 3D left coronary artery bifurcation model decreases with increasing bifurcation angle and the time-averaged inlet pressure is the least for smaller bifurcation angles. The current research further concentrates that the flow separation length reduces with developing bifurcation angle in bifurcated geometry. It is significant to mention that non-Newtonian blood flow model incorporating hemodynamic and diagnostic parameters has great impacts on instantaneous flow systems.

1. Introduction

Atherosclerosis begins by damaging the endothelium layer in the artery. Atherosclerosis, a dangerous cardiovascular disease of long and moderate-shaped vessels, where lipids, cholesterol, fat and other substances deposit in the endothelium of the inner layer of usual blood vessels building plaques. Since lipids called plaque develop with varying time which causes a partial reduction of artery cross-section. These constrictions or blockage has an elaborate impact on the flow of blood through as well as after the constricted part of the blood vessel. The probability that hemodynamic parameters can involve to generation and enlargement of atherosclerosis has brought up developing the flow research through the stenotic artery during the period of past years. The improvement of flourished atherosclerotic buildup plaques may appear preferably in elevated shear regions is consecrated to us. From the fluid flow analysis

* Corresponding author. Department of Applied Mathematics, University of Dhaka, Dhaka-1000, Bangladesh
E-mail address: zavid@du.ac.bd (M.Z.I. Bangalee).

https://doi.org/10.1016/j.heliyon.2023.e17533
Received 26 January 2023; Received in revised form 31 May 2023; Accepted 20 June 2023
Available online 3 July 2023

viewpoint, it is advantageous to investigate and locate the regions of high shear as well as flow normal stresses, extremely low or the areas where the shear stress appears extremely high at the lesion of atheromatous walls and the extension areas where flow reverse in cardiovascular arterial blood vessels.

Numerical Computation to the steady blood flow through a rigid wall of stenotic artery has been investigated on hemodynamics and showed well-matched comparison of outcomes with experimental results [1]. Different stenosis severities associated with atherosclerosis have impacts on hemodynamic parameters for left anterior descending coronary artery [2]. The results indicate that there are great changes in hemodynamics between the stenosis of 60 and 70%. The variation of hemodynamics can be used in the clinical sector. The hemodynamic factors like, time-averaged wall shear stress (TAWSS), oscillatory shear index (OSI), relative residence time (RRT) related to endothelium damage with thrombus deposition and non-Newtonian importance factors such as local non-Newtonian importance factor (I_L), global non-Newtonian importance factor (I_G), non-Newtonian effect factor (NNEF) are most important to describe vascular flows for 3D bifurcation [3]. The RRT factor is connected with the blood particles residence time across the vessel wall and can be used for detecting the regions which are susceptible to atherosclerosis. This RRT method is compared with blood residence time (RT) method [4]. It is found that the method has ability to display the separation zone in the artery lumen and also susceptible to quantify real RT. A 3D bifurcated left coronary artery model has been utilized with double constriction to capture the blood hemodynamics [5]. It is observed that non-Newtonian model has impacts on blood flow in the lumen for the blockage intensity of 90%.

According to the previous research, the blood flow issue has been divided into two characters, namely, Newtonian and non-Newtonian fluid. Following various blood models, the impacts of artery wall elasticity, flow of blood with heat transfer, fluid particle transport are investigated [6–8]. Since blood consists of blood cells and plasma and generally approaches as a Newtonian fluid. Nevertheless, in accordance with the blockage artery conditions, blood should be considered as a non-Newtonian nature [9]. Though doctors use diagnostic parameters as a practical purpose, the application has not been well established in early studies. The general diagnostic parameters [10,11] are fractional flow reserve (FFR), pressure drop coefficient (CDP) and lesion flow coefficient (LFC) which have common application. Numerical simulations of an oscillating flow past in the conduits of plane through the wall obstacles of the square have been reported by investigator [12]. Such outcomes are of eminent gusto as the pulsatile flow area is employed. Liao et al. [13] have studied a bell-shaped constriction for three various patterns of flows of pulsation and decided that the perturbations of characteristic flow parameters influence the flow area in case of physiological flow. Halder et al. [14] have discussed the comparative analysis between Newtonian and non-Newtonian fluids through a stenotic vessel. Razavi et al. [15] have numerically investigated the flow dynamics through an axisymmetric common carotid stenotic artery varying blockage intensity 30 – 60% under Newtonian and non-Newtonian blood rheological models.

A numerical investigation may have great impacts on the essentiality of applying patient-specific inflow velocity profiles to examine the thoracic aorta disease states using finite element method [16]. The WSS topological skeleton conducts the near-wall biochemical transport through the arteries and it plays a key role in, e.g., the inception of atherosclerosis and thrombogenesis [17]. In 3D bifurcated carotid artery, the hemodynamic changes have been investigated for the bifurcation angle of symmetric and asymmetric due to steady and pulsatile flow. The simulated results reveal the significant difference in behavior between steady and pulsatile flow [18]. Lakzian et al. [19] have studied the Newtonian and non-Newtonian unsteady blood pulsatile flow in a 3D curved stenotic artery. The findings point out that the maximum wall shear stress occurs at the neck of the blockage. Abbas et al. [20] have numerically investigated the pulsatile blood flow through an arterial overlapping stenotic blood vessel under the action of periodic body acceleration. The Sutterby fluid model characterizes the blood rheology. The software, COMSOL Multiphysics [21] is used for solving the set of governing equations, subject to the corresponding boundary conditions.

Hence, in the present research, the most well-known blood constitutive equation namely, the Carreau model as a non-Newtonian fluid has been activated in an attempt to examine the blood pulsatile flow through the stenotic and bifurcated left coronary artery. A numerical model of arterial blood flow is induced for two-dimensional (2D) and 3D bifurcated geometry to give the idea about the hemodynamic changes, to provide clinical diagnosis treatment and to establish a comparison between Newtonian and non-Newtonian fluid. The non-Newtonian importance factor has also provided a new concept for arterial flows.

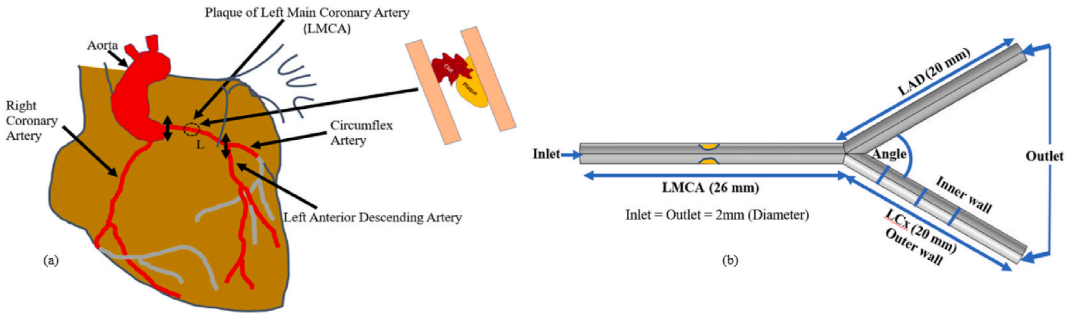

Fig. 1. (a) Human realistic coronary artery (b) Left coronary bifurcation model used in the study.

2. Numerical methodology

The symmetric bifurcation model has been considered here with same diameter of 2 mm [22] for left main coronary artery (LMCA), left circumflex artery (LCx) and left anterior descending artery (LAD) in Fig. 1(a and b). The length of main coronary artery is 26 mm [13] and each branch artery is 20 mm. To investigate in details of left coronary bifurcated artery, the two parts have been assumed due to Newtonian and non-Newtonian fluid.

A reasonable numerical solution for the rheological blood flow models is obtained by following several systematic steps related to CFD as follows:

2.1. Computational domain for 2D stenotic and 3D bifurcated coronary artery

The arterial geometry with the symmetrical stenosis and bifurcated geometry are captured for numerical investigation as presented in Fig. 2(a) and (b), respectively. The coordinates (r, z) for 2D has been taken as a cylindrical coordinate system and z axis is situated along the symmetric axis of the LMCA. In 3D bifurcated geometry, the diameters of mother and daughter vessels are of 2 mm.

The profile of stenosis can be defined mathematically using the following formula [13] in Eq. (1):

$$\frac{\mathrm{r}}{\mathrm{r}_0} = 1 - \frac{\mathrm{h}}{2\mathrm{r}_0}\left(1 + \frac{\cos \pi \mathrm{z}}{\mathrm{z}_0}\right) \tag{1}$$

$$z_0 \geq z \geq -z_0$$

where r, artery radius with the function of z at blockage area, L, artery length and r_0, unblocked artery radius. In present investigated case, $h = 0.5$ and $z_0 = 1$ [13].

2.2. The governing equations and boundary conditions for 2D and 3D bifurcated artery

Governing equations can be written for the models of 2D and 3D as follows:

Continuity equation: The Continuity equation becomes

$$\rho \nabla . u = 0 \tag{2}$$

Momentum equation: The momentum equation yields

$$\rho \frac{\partial u}{\partial t} + \rho (u . \nabla) u = \nabla . \left[- pI + \mu \left(\nabla u + (\nabla u)^T \right) \right] + F \tag{3}$$

Where ρ indicates the density (kg/m^3); u, vector of velocity (m/s); p, pressure (Pa); I, identity matrix and the volume force vector is F (N/m^3). Eq. (2) is the continuity equation and represents the conservation of mass. Eq. (3) is the vector equation and indicates the conservation of momentum. Blood density is varied within the range $1030 - 1070$ (kg/m^3) [23] based on age and sex. For conservative analysis, the main and daughter arteries (3D) diameters of 0.2 cm each are taken together with the blood properties of 0.00345 $Pa.s$ for the dynamic viscosity to Newtonian fluid and the blood density of 1.05 g/cm^3 is assumed for Newtonian and non-Newtonian fluid. The flow analysis has been carried out for both Newtonian and non-Newtonian fluids. The non-Newtonian properties stated here and computational results are validated by Halder et al. [14]. The dynamic viscosity for the Carreau-Yasuda model as non-Newtonian fluid is expressed in the following Eq. (4):

$$\mu = \mu_\infty + (\mu_0 - \mu_\infty) \left[1 + (\lambda \dot{\gamma})^2 \right]^{\frac{n-1}{2}} \tag{4}$$

Here, viscosity of low shear, $\mu_0 = 0.056$ Pa.s, viscosity of high shear, $\mu_\infty = 0.00345$ Pa.s, constant of time, $\lambda = 3.3313$ s, index of power law, $\mathrm{n} = 0.3568$, exponent of Yasuda, $a = 2$ [24]. The Carreau-Yasuda model exists continuity for the higher range of flow shear rates $(\dot{\gamma} \geq 0)$. The fluid viscosity approaches to the value of μ_∞ at high shear thinning and approaches to μ_0 at low shear thinning that mimics creditably blood flow modeling [15,24,25]. In this study, two familiar velocity profiles namely, simple pulsatile and equivalent pulsatile flows are employed to investigate the flows in artery. The cyclic variations of velocities are shown in Fig. 3(a). The simple pulsatile flow is the sinusoidal waveform in Eq. (5) and equivalent pulsatile flow is formulated according to Ref. [26] and indicated as

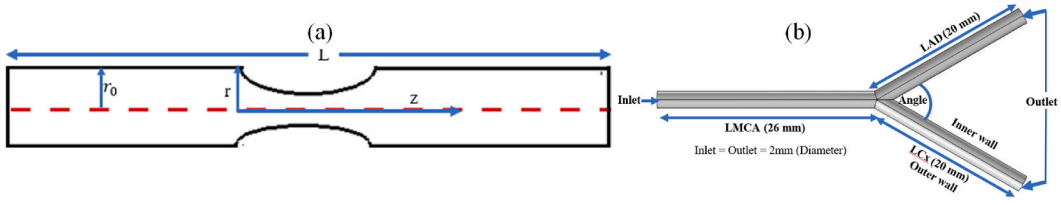

Fig. 2. (a)2D stenotic and (b) 3D bifurcated coronary artery in the present study.

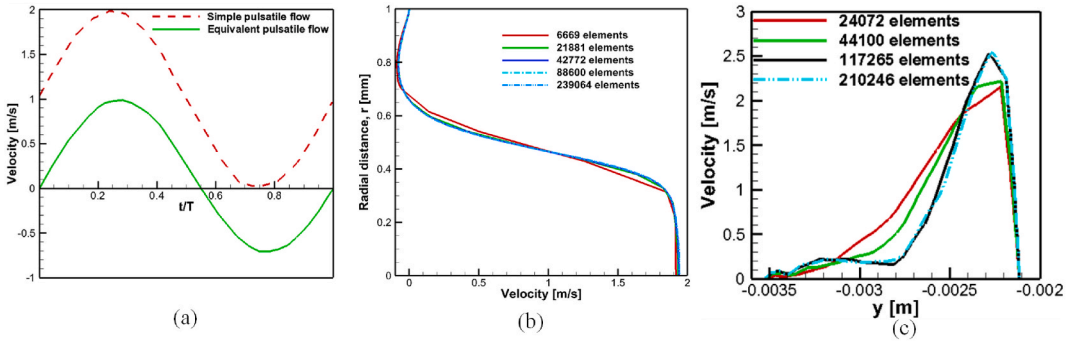

Fig. 3(a). Simple and equivalent inlet velocity profiles (b) Velocity profile along r for different grids in 2D and (c) Grid test for 3D bifurcation.

Eq. (6):

Simple pulsatile flow:

$$u_z(t) = 1 + \sin\left(2\pi \frac{t}{T}\right) \tag{5}$$

Equivalent pulsatile flow:

$$u_z(t) = 1 - \alpha\left(1 + \cos\left(2\pi \frac{t}{T} + \varphi\right)\right) \tag{6}$$

Where time period is T, amplitude is α and phase angle is φ. No slip boundary condition is used for the wall of a rigid artery and unsteady velocity is imposed at inlet. The outlet boundary conditions of the main and bifurcated branch arteries are subjected to 0 Pa. The pulse period of these waveforms is 1 s which represents the actual heart rate of 60 beats / min of a human.

2.3. Numerical solution for 2D and 3D bifurcated geometry

The actions regarding the modeling, meshing and computing all of them have been executed with COMSOL Multiphysics for 2D and 3D bifurcated coronary artery. In this research, the finite element method is employed to solve the set of equations. The simulated geometry is meshed in the unstructured based on finite element method. The solver methods have chosen the implicit backward differentiation formula (BDF) for the solution. The convergence criterion is set to 10^{-4}. The simulation is performed for the time step of $\Delta t = 0.01\ s$, $\Delta t = 0.001\ s$ and $\Delta t = 0.0001\ s$ for making time step independency but there are no significant changes so that's why the time step of $\Delta t = 0.001\ s$ has been taken. To make secure the periodic outcomes, the numerical simulations are conducted for two pulsatile cycles but there is no change and the first cycle is taken for the simulation of predicted results due to convenience.

2.4. Grid independency test for 2D and 3D bifurcation geometry

The grid generation tool COMSOL Multiphysics is operated to develop the grid for the computational domain. The mesh dependency test is carried out to assure the predicted results which are not dependent on the mesh parameters. Several attempts have been made but only five of them will be stated here. The number of domain elements, domain boundaries and degree of freedom for each 2D mesh test is summarized in Table 1. From each of the mesh, the results of velocity magnitude are evaluated and graphically shown in Fig. 3(b). The number of mesh elements are grown softly from mesh 1 (6669) to mesh 5 (239064) to examine the grid dependence of the solution. The computed results indicate that there is small alters between the numerical results particularly contribution to mesh 1 and mesh 3. The velocity magnitude from mesh 4 to mesh 5 at the axial distance Z = 1 [mm] for t = 0.6 s is approximately the same. Therefore, we have been decided that the parameters quantities of mesh 4 are sufficient to provide accurate solutions to the problem. The velocity magnitude gained for four various meshes at a distance of 2D from bifurcation point on the daughter LCx plane is plotted in Fig. 3(c) for 3D bifurcated geometry. There is no significant difference in velocity magnitudes for the last two mesh elements 117265 and 210246. Hence, the mesh comprising 117265 elements has been taken for the numerical

Table 1
Mesh parameters for 2D geometry of arterial stenosis.

Parameter	Domain Elements	Boundary Elements	Degree of Freedom
Mesh 1	6669	615	12109
Mesh 2	21881	1177	36844
Mesh 3	42772	1570	69337
Mesh 4	**88600**	**2834**	**143218**
Mesh 5	239064	4952	377791

computations. The computational mesh of the 2D stenotic artery of the model around the blockage area in the current investigation as displayed in Fig. 4.

2.5 (see). Fig. 5Methodology validation for 2D and 3D bifurcated geometry

The steady narrate that fully developed flow area is propagated through numerical simulations and the enumerated outcomes are compared with Newtonian and non-Newtonian fluids. The velocity distributions are also of gusto since they contribute a clear assertion of the flow field. We first carry out the numerical simulation through a 75% stenosis with Reynolds number Re = 200 in a rigid tube. Fig. 5(a) presents axial velocity distributions at various axial locations ($Z = 0, 1, 10.26$) for Re = 200 to Newtonian fluid. The axial locations and the Reynolds number are selected such that analogies can be created with the simulated results of Deshpande et al. [1], Liao et al. [13]. The velocity profile turns out much beefier at the stenosis throat ($Z = 0$) than at the ingress. Slightly downstream ($Z = 1$) from the throat location, the velocity exhibits a recirculation zone near the wall and it disappears at $Z = 10.26$. These comparisons are employed to validate the 2D stenotic method with maximum error of 4.48% and minimum error of 0%.

Fig. 5(b) also displays the axial velocity at the positions of Z = D and 6D from bifurcation point for non-Newtonian fluid to validate the method of 3D bifurcation. At daughter locations, the model is also justified by non-Newtonian fluid for bifurcation symmetric angle ($\alpha = \beta = 30^o$) with Nagargoje et al. [27] for a maximum error of 2.04% and minimum error of 0%. These velocity distributions assimilate beyond a doubt with the gained by Deshpande et al. [1] Liao et al. [13] and Nagargoje et al. [27].

The radial velocity is estimated by the current technique of 2D in strong consent with the literature profiles without slight detachment for the axial positions $Z = 0, \pm 0.3$ and $Z = \pm 0.52$ in Fig. 6 with a maximum error of 1.33% and minimum error of 0%. At $Z = -0.3,$ it is approximately 11.5% larger than the mean velocity in unblocked tubes which is slightly lower than the actual reference of Deshpande et al. [1] in the present case. The recirculation presents here for the axial and radial velocity which is satisfied with the literature.

A thin boundary layer of a flowing fluid of viscous relative to a close artery wall surface in contact with the stream of moving in which the velocity of the flow varies within zero (no slip boundary wall) and free stream velocity. The theoretical estimations of boundary layer thickness (δ) for simple and equivalent pulsatile flows are 0.41 mm and 0.55 mm, respectively which are also identified in the present study for fully developed flow in the unobstructed artery section, indicating a performance of the CFD code for 2D and shown in the following Fig. 7.

2.6. Hemodynamic and diagnostic indices concerning the investigation need to be concentrated

According to the governing equations, Stress tensor in Eq. (7) is

$$\tau = \mu\left[\nabla u + (\nabla u)^T\right] \tag{7}$$

Where μ indicates the dynamic viscosity and T is the transpose. The viscosity μ will be a constant, if the blood is acted as a Newtonian fluid. However, the real blood consisting of blood cells and plasma, which behaves rheologically. In this study, the non-Newtonian shear-thinning effects are predicted by the Carreau-Yasuda model according to the above Eq. (4).

Pressure drop (Δp): The pressure drop between pre-stenosis proximal and post-stenosis distal in Eq. (8) can be expressed as

$$\Delta p = p_a - p_d \tag{8}$$

Where p_a is the pre-stenosis proximal pressure and p_d is the post-stenosis distal pressure.

Coefficient of pressure drop (CDP): The non-dimensional index, CDP is the ratio of pressure drop through the blockage to the dynamic pressure at distal and which is the combination of pressure and measurements of flow [28]. It can be stated as the following Eq. (9):

$$CDP = \frac{\Delta\overline{p}}{0.5\rho\overline{U}_p^2} \tag{9}$$

$\Delta\overline{p} = \overline{p}_{proximal} - \overline{p}_{distal}$, $\Delta\overline{p}$ represents the difference of time-averaged pressure between proximal and distal site. $\overline{U}_p$ indicates pre-stenosis time-averaged velocity at proximal.

Coefficient of lesion flow (LFC): The LFC in Ref. [11] can be identified as the ratio of area blockage in percent to the square root of

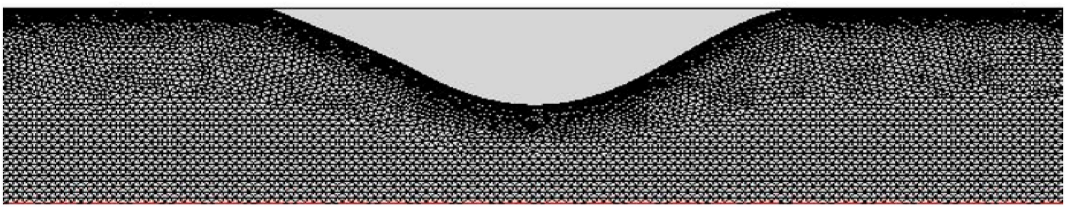

Fig. 4. The computational mesh of 2D around the stenosis site.

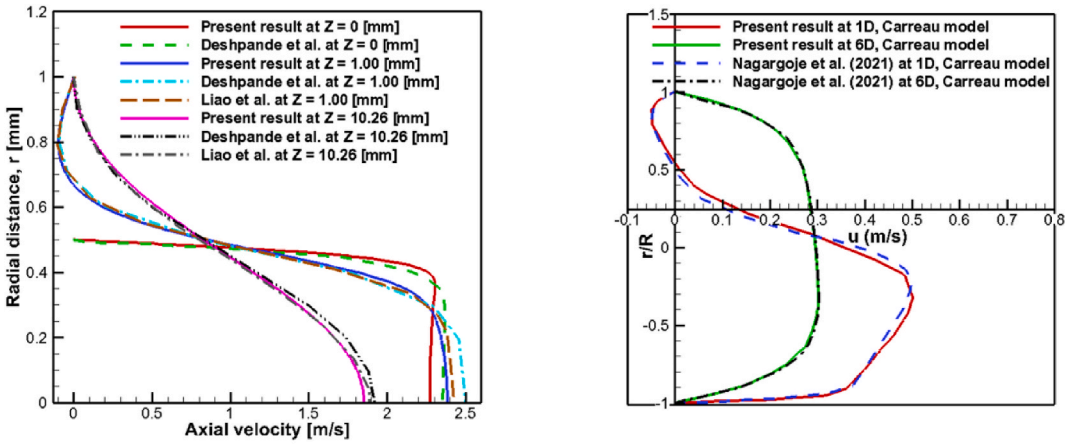

Fig. 5. CFD comparison between predicted results and Deshpande et al. [1], Liao et al. [13] and Nagargoje et al. [27] for axial velocity on various locations for Newtonian and non-Newtonian fluid.

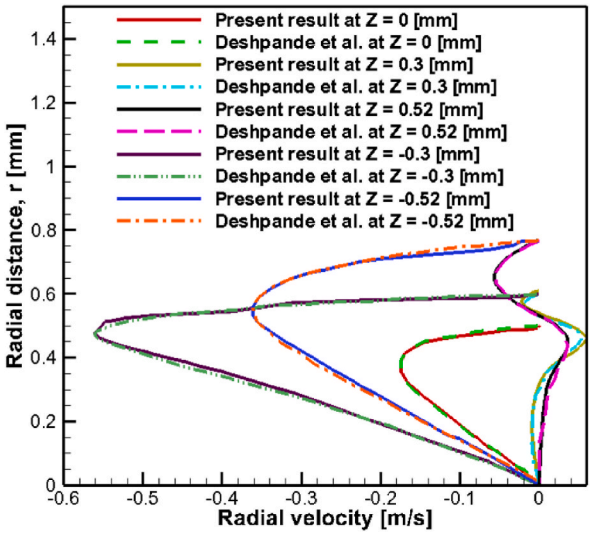

Fig. 6. Validation of the present numerical method with the simulated predictions [1] at various axial locations for the radial velocity of Newtonian fluid.

CDP in the region of throat which describes the anatomical and functional measurements and given as Eq. (10)

$$\mathrm{LFC} = \frac{AS}{\sqrt{\frac{\Delta\bar{p}}{0.5\bar{\rho}\bar{U}_{d-h}^{2}}}} \tag{10}$$

Where $AS = \frac{\pi\left(\frac{d}{2}\right)^2 - \pi\left(\frac{d}{2}-h\right)^2}{\pi\left(\frac{d}{2}\right)^2}$, $\overline{U}_{d-h}$ indicates the time-averaged velocity at constriction site.

3. Results and discussion

A. 2D Left Main Coronary Stenotic Artery

The study of the two-dimensional axisymmetric blood flow simulation is conducted depending on the available literature result suggested by Deshpande et al. [1] and Liao et al. [13] as mentioned in the previous section. The main purpose of this discussion is to investigate the blood flow behaviors, streamlines pattern and LFC for two flows and the effect of stenosis severity on this blood flow

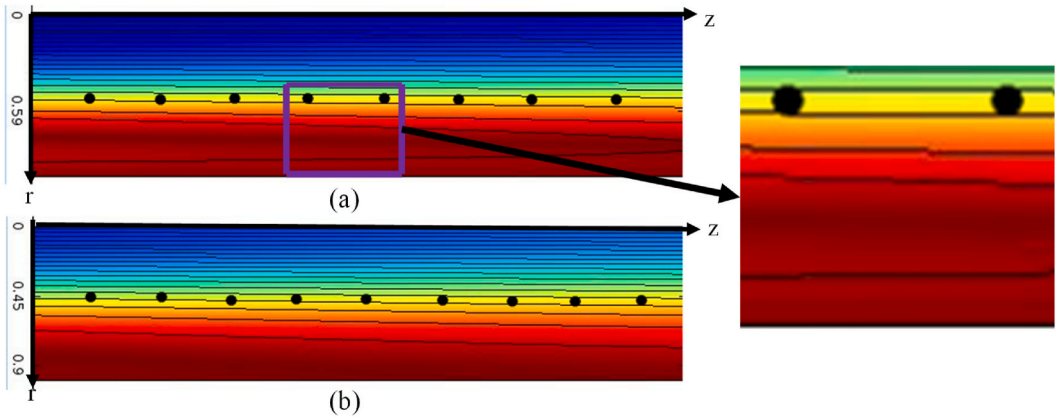

Fig. 7. Boundary layer thickness for (a) simple and (b) equivalent pulsatile flow.

characteristic. All simulated results are carried out according to stenosis profile except for Fig. 21(a and b), Fig. 23(a and b), Fig. 24(b) & Fig. 25(a and b).

3.1. *Velocity distribution at various axial locations*

For the investigated internal flow, the analysis of the transient flow is driven for Newtonian and Carreau model due to both pulsating flows and is observed the flow characteristics at the axial $(Z = -8, -4, 0, 4 \text{ and } 8 \text{ mm})$ positions of artery are assimilated as displayed in Fig. 8(a and b) & 9 (a, b). A lower velocity magnitude from upstream develops, and higher velocity exists at Point C for the stenosis throat and at D for the proximal downstream to stenosis compared to the upstream positions for both velocity profiles of the Newtonian (Figs. 8(a) and Fig. 9(a)) and non-Newtonian fluid (Figs. 8(b) and Fig. 9(b)) by dint of arterial blockage. But the velocity is decreasing as the distance increasing from the stenosis throat to the downstream location of the artery. The highest velocity appears at the proximal downstream to vessel constriction for Newtonian and Carreau viscosity models. The velocity whose shape in the inlet corresponds to sinusoidal laminar pulsatile flow, rises near the stenosis neck and specially at proximal stenosis downstream most. It then falls at the downstream positions for the cases.

For equivalent pulsatile flow (Fig. 9(a) and (b)), the maximum velocity appears at constriction and post constriction regions during the pulse of forward and it is customarily identical to inlet simple flow pulsation, whereas the position of maximum velocity (u_{max}) is moved towards upstream portion at the time of backward pulse. The maximum magnitude of velocity (u_{max}) is observed at Point C and D for throat and proximal post-stenotic areas, respectively for all investigated cases. But the significantly highest velocity is noticed at proximal downstream than the middle of the stenosis for the two fluids. The maximum velocity (u_{max}) also appears for the flows at the

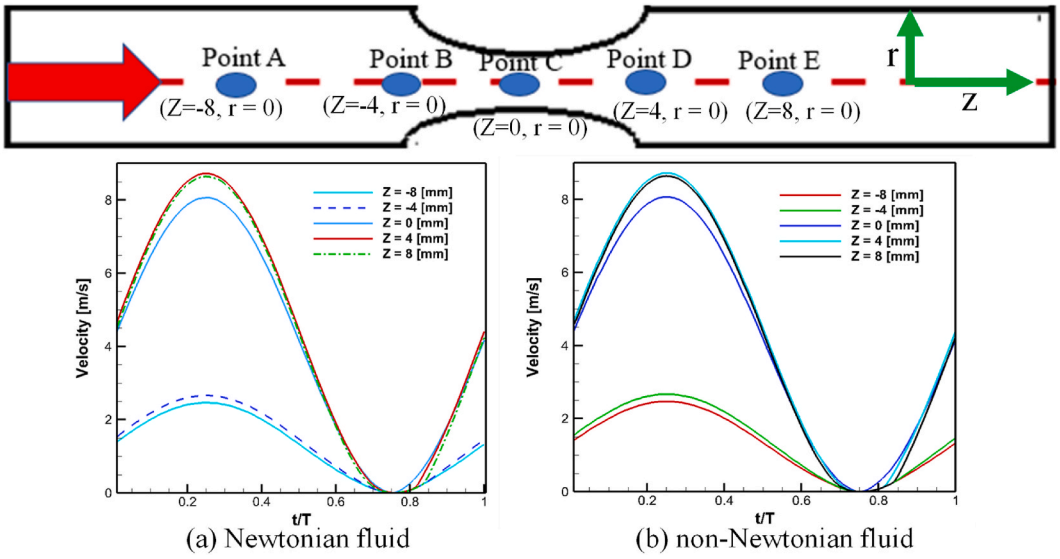

Fig. 8. Velocity distribution for simple pulsatile flow at various axial locations (where r = 0) for (a) Newtonian and (b) non-Newtonian fluid.

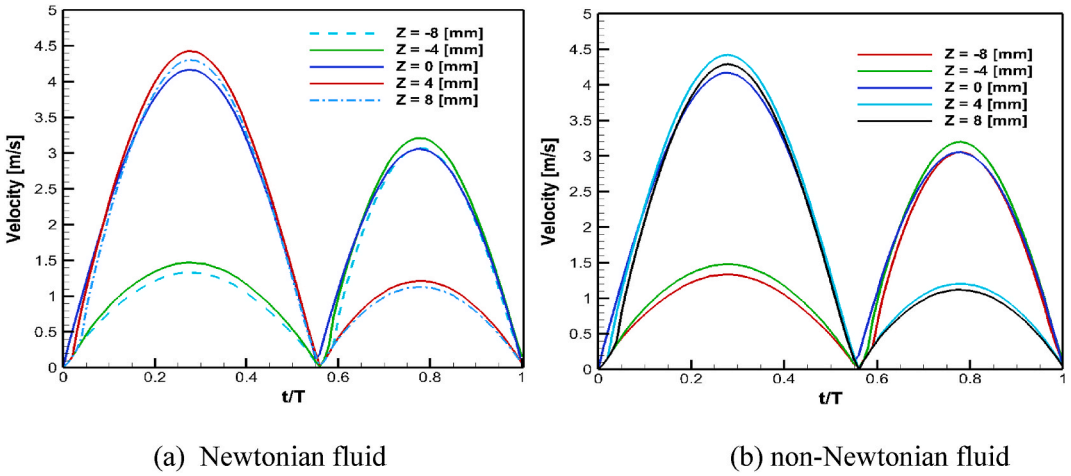

Fig. 9. Velocity distribution for equivalent pulsatile flow at various axial positions for (a) Newtonian and (b) non-Newtonian fluid.

time interval $3T/10$ through the forward pulse for two models. The minimum magnitude of velocity $(u_{min} = 0)$ is viewed at every point at various time intervals, that is at $0.7 * T$ for simple pulsatile flow (Fig. 8(a) and (b)) and at $0 * T, 0.55 * T$ and T for equivalent pulsatile flow (Fig. 9(a) and (b)).

3.2. Pressure distribution at different axial positions

The blood pressure in maximum arteries is unsteady and over specifically it is pulsatile in behavior which creates variation in blood pressure pattern during various periods. The cyclic characteristics of the heart pump generate pulsatile conditions in all types of arteries. The heart ejaculates and saturates with blood in interchanging cycles called systole and diastole. Through the systole blood is pumped out of the heart. At diastole, the heart rests and causes ejection to no blood. The pressure increases at the upstream side of the severe stenosis and reaches to throat location to around zero at the time interval $7T/10$ in case of simple pulsatile flow (Fig. 10(a) & Fig. 10(b)). The smaller pressure values are noticed at the location of the stenosis throat (Point C) in the current investigation, and also the smallest pressure value is seen at the proximal downstream (Point D) location which is negative at the time interval $0.3T$. The maximum pressure values are observed at the pre-stenosis side for both Newtonian (Fig. 10(a)) and non-Newtonian fluid (Fig. 10(b)) for the simple pulsatile flow at the time interval $0.3T$, and appear larger in Newtonian fluid. In case of accelerating phase of the systole in the pre-stenosis location, the pressure is large, the pressure flops near zero at $t = 0.55$ s (Fig. 11(a) and (b)), and it goes rapidly in the negative due to the reverse direction of the inflow and the maximum and minimum values of the pressure are found at the time intervals $0.3T$ and $0.75T$ for the Newtonian (Fig. 11(a)) and non-Newtonian (Fig. 11(b)) equivalent pulsatile flows. It is concluded that the highest value of the simple and equivalent pulsatile flow is investigated at the same time $0.3T$ on the pre-stenosis location for the Newtonian fluid.

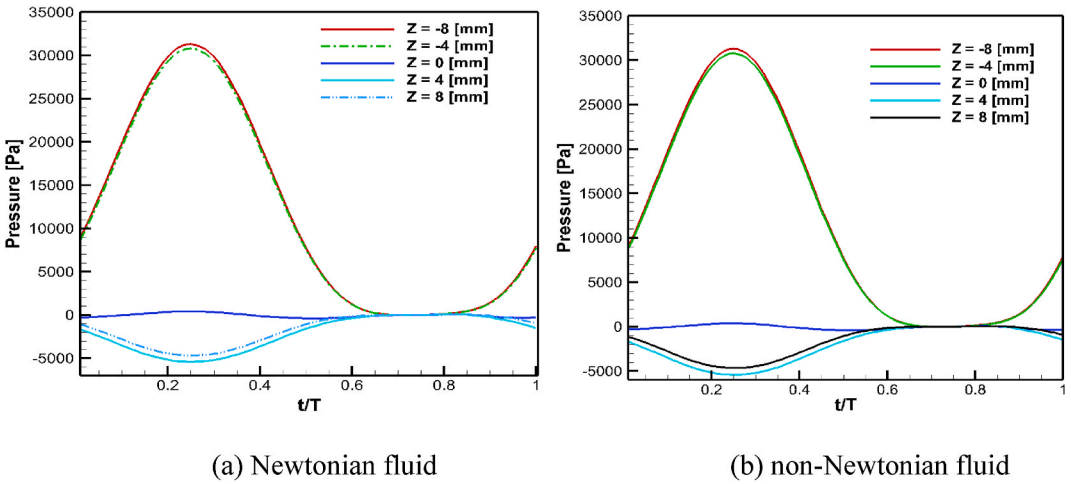

Fig. 10. Pressure distribution at various locations for (a) Newtonian and (b) non-Newtonian simple pulsatile flows.

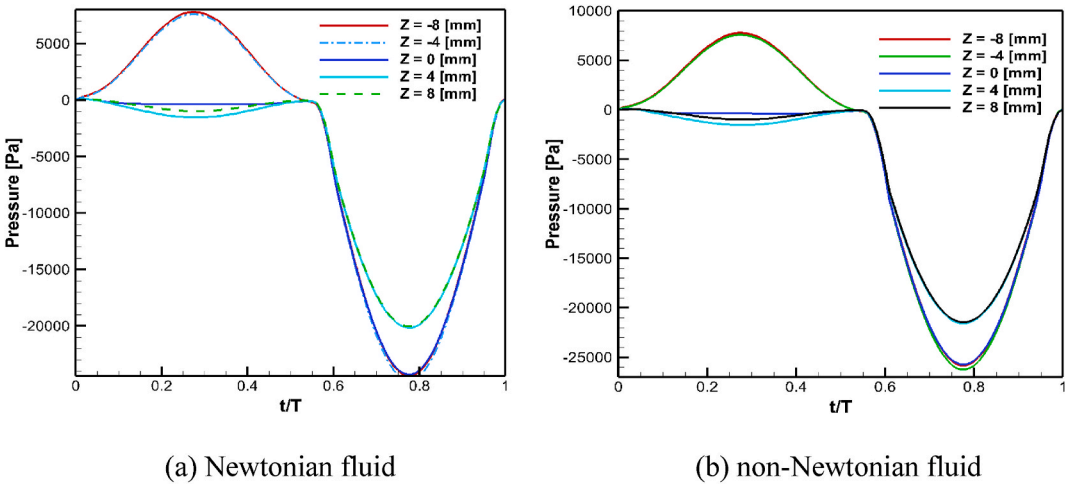

Fig. 11. Pressure distribution of (a) Newtonian and (b) non-Newtonian fluid on various locations for equivalent pulsatile flow.

3.3. Effect of inlet velocity pulse on centerline velocity and pressure for simple pulsatile flow

The impact of the unsteady inlet pulse of velocity on the arterial flow field is investigated thoroughly in the distribution of velocity and pressure towards the arterial symmetric axis at different time instants for simple pulsatile flow (Fig. 12(a) & Fig. 12(b)). The

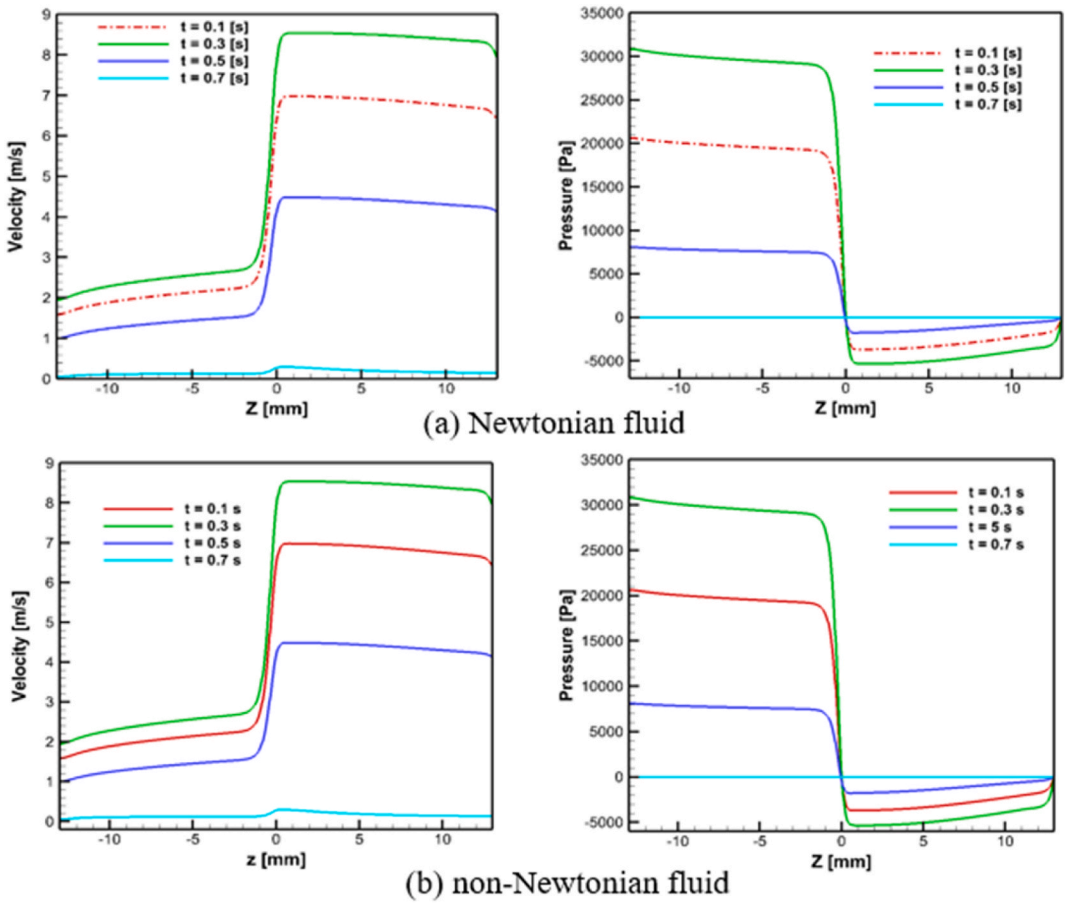

Fig. 12. Velocity and pressure distribution for simple pulsatile flow along the arterial centerline at several time intervals for (a) Newtonian and (b) non-Newtonian fluid.

velocity grows softly along the way of the flow until the stenosis throat and strongly around the stenosis of the artery. Moreover, velocity reduces slowly at the downstream region until the artery end. The highest and the lowest velocity occur in the artery at $t = 0.3\,s$ and $0.7\,s$, respectively for simple pulsatile flow (Fig. 12(a) (left) and Fig. 12(b) (left)). The peak value of velocity in the non-Newtonian case (Fig. 12(b) (left)) is negligible higher than in the Newtonian case (Fig. 12(a) (left)).

The pressure distribution complies velocity of flow as hoped. In the pre-stenosis location pressure spill is linear signifying fully developed flow circumstances for both Newtonian (Fig. 12(a) (right)) and non-Newtonian fluids (Fig. 12(b) (right)). As the blood flow approaches to stenosis neck, the local pressure minimizes because of the flow acceleration in the narrowing part, and it is then succeeded by gradually rise until the artery end. The lowest pressure exists at $t = 0.3$ s in the proximal post-stenosis region for Newtonian and non-Newtonian fluids indicating the regime prone to atherosclerotic process which is compared and shown in Fig. 12(a) (right) & Fig. 12(b) (right). If the degree of stenosis is very high, the pressure at the stenosis neck may be smaller than the external pressure, and consequently the stenosis may collapse, causing chocking of flow and likely leading to heart attacks.

3.4. *Effect of inlet velocity pulse on centerline velocity and pressure for equivalent pulsatile flow*

Also, the distribution of velocity and pressure along the arterial centerline are observed for Newtonian and non-Newtonian fluid of the equivalent pulsatile flow at several time intervals and are exhibited in Fig. 13 (a) & Fig. 13(b). The peak velocity at $t = 0.3$ s for the Newtonian fluid (Fig. 13(a) (left)) is slightly difference compared to the highest velocity for the non-Newtonian fluid (Fig. 13(b) (left)), and the lowest velocity $(u_{min} = 0$ approximately$)$ happens at $t = 0.55$ s (Fig. 13(a and b) (left)) for both fluids. Blood flow and pressure are unsteady and they have the nature of pulsatile patters which vary in the arterial system. The maximum pressure appears at upstream locations of stenosis at $t = 0.3$ s and the pressure approximately zero at $t = 0.55$ s for both Newtonian (Fig. 13(a) (right)) and non-Newtonian fluids (Fig. 13(b) (right)) in case of equivalent pulsatile flow, and causing a little difference between the two fluids. The pressure drop is higher in the period of $t = 0.3 * T$ in the Newtonian case (Fig. 13(a) (right)) than the non-Newtonian case (Fig. 13(b) (right)) for equivalent pulsatile flow. It is remarkable that the maximum pressure for both flows is larger in the Newtonian fluid.

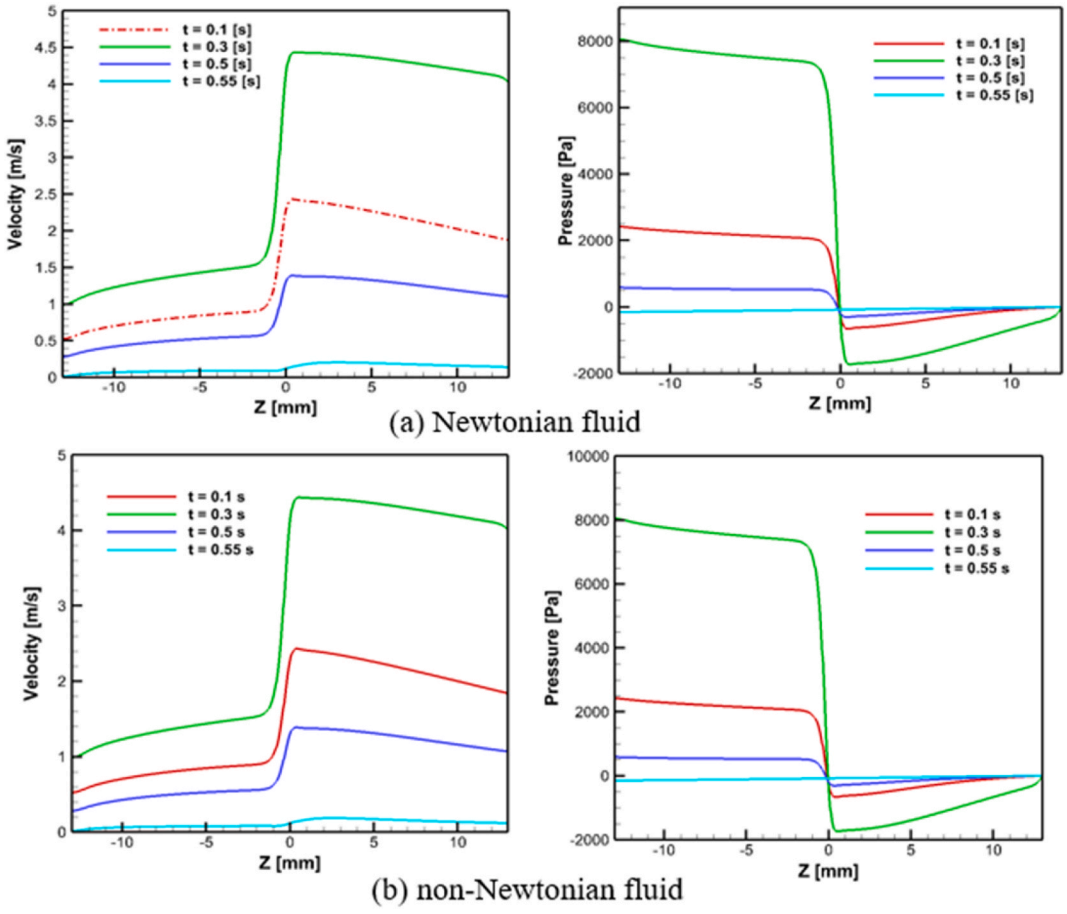

Fig. 13. Distribution of velocity and pressure along the arterial centerline for (a) Newtonian and (b) non-Newtonian fluid at several time intervals of equivalent pulsatile flow.

3.5. Evaluation of shear stress and shear rate for both fluids of simple pulsatile flow

Another gusto of hemodynamic is the impact of the blood flow attitude on the shear stress since it is well accepted that shear stress is a cabalistic factor in the commencement of arterial diseases. Elevated shear stress in the partly blocked vessel has been known to actuate platelet-platelet binding cases that play a great significant role in the case of thrombosis. The shear stress and shear rate along the symmetric axis through the artery with a severe stenosis considering several time intervals of a cycle have been evaluated in this paper for the Newtonian and non-Newtonian fluids for two inlet flows as displayed in Fig. 14 (a, b) & Fig. 15(a and b). At first sight over the figure, it is undoubtedly noticed that all the fluids succeed same patterns, and the peak value of shear stress appear at the stenosis throat. A significant allusion is that the maximum shear stress exists during the peak systole at $t = 0.3$ s (Fig. 14(a and b) (left) & Fig. 15 (a and b) (left)) for all the cases. While the minimal shear stress is investigated at $t = 0.7$ s for the simple pulsatile flow (Fig. 14(a and b) (left)) and at $t = 0.55$ s for the equivalent pulsatile flow (Fig. 15(a and b) (left)) for both models.

3.6. Shear stress and shear rate for both fluids of equivalent pulsatile flow

Under the severe stenosis, the shear stress of the non-Newtonian fluid (Fig. 14(b) (left) & Fig. 15(b) (left) is greater than that of the Newtonian fluid (Fig. 14(a) (left) & Fig. 15(a) (left) specially, for the maximum flow phase $(t = 0.3 * T)$ but both have similar trends. Therefore, the stenosis of the artery actually causes a noteworthy shear stress increase. Indeed, the high-speed flow at the stenosis location consequences in the elevated shear stress, and clinically, this location may be the fibrous cap in the considered vessel. The homologous mechanical stress may respond to plaque rupture and unfastened material. Fig. 14(a and b) (right) & Fig. 15(a and b) (right) also show the shear rate distribution at several time intervals $(t = 0.1 * T, 0.3 * T, 0.5 * T, 0.7 * T)$ and ($t = 0.1$*T, 0.3*T, 0.5*T, 0.55*T) of the simple and equivalent pulsatile flow, respectively for Newtonian (Fig. 14(a) & 15(a) (right)) and non-Newtonian fluid (Fig. 14(b) (right) & Fig. 15(b) (right)) through the pulsatile cycle. An elevated shear rate is occurred at the maximum flow rate $(t = 0.3 * T)$ for the Newtonian blood viscosity model in the case of simple and equivalent pulsatile flows.

3.7. Wall vorticity distribution for two flows of both fluids

The vorticity is of physiological significance as it is commensurate with shear stress that is once and again applied as exhibitor

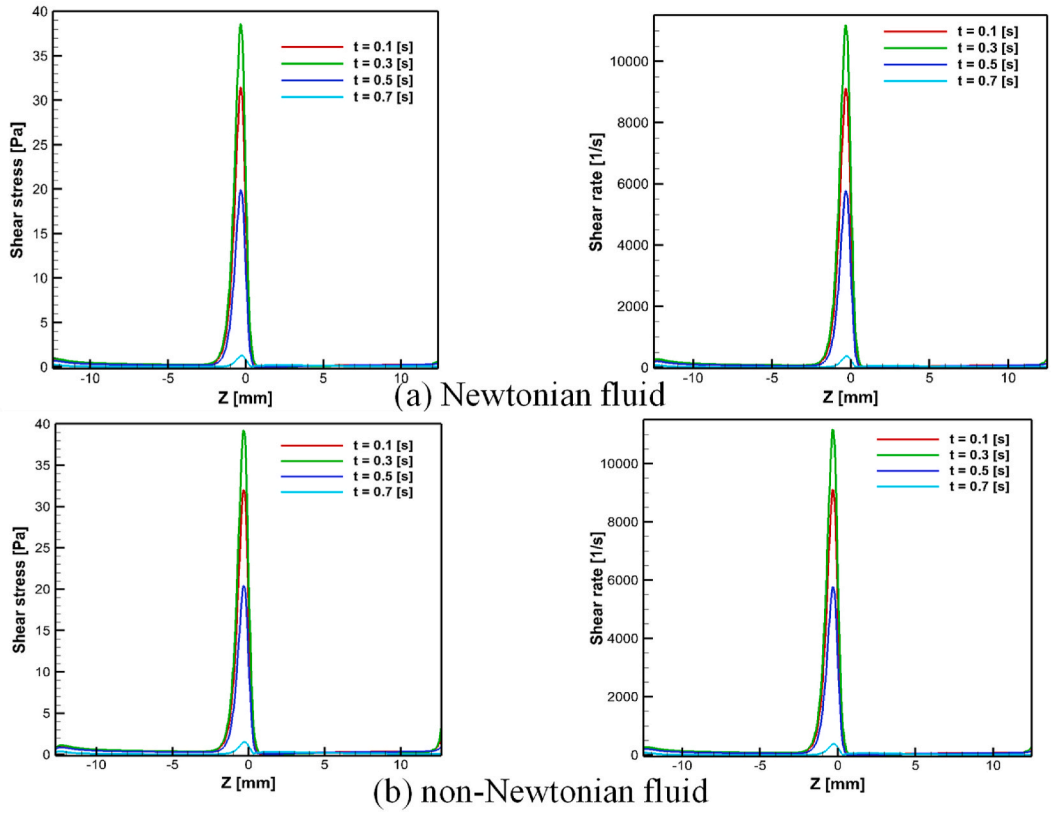

Fig. 14. Shear stress and shear rate distributions along the arterial centerline for (a) Newtonian and (b) non-Newtonian fluid at various time intervals for simple pulsatile flow.

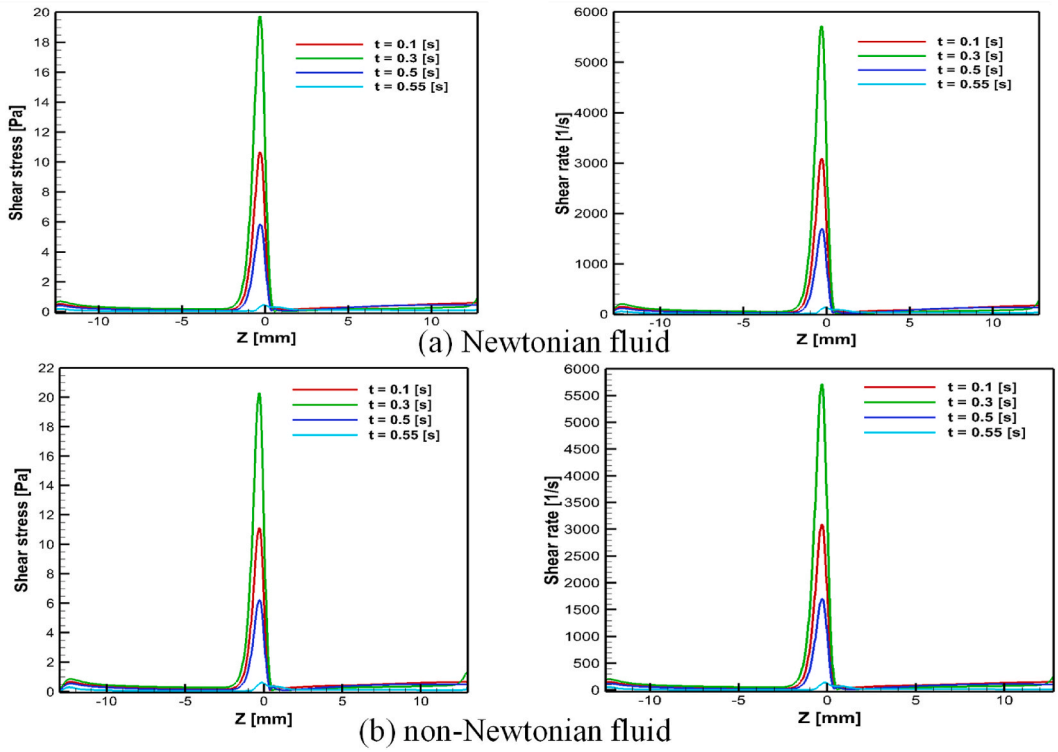

Fig. 15. Shear stress and shear rate distributions along the arterial centerline for (a) Newtonian and (b) non-Newtonian fluid at various time intervals of equivalent pulsatile flow.

functions for the commencement and betterment of arterial diseases. It can be observed that the vorticity grows up speedily and attains its maximum value near the stenosis for Newtonian (Fig. 16(a) and Fig. 17(a)) and non-Newtonian viscosity model (Figs. 16(b) and Fig. 17(b)) for two inlet velocity profiles. Clearly, the larger instantaneous flow rate causes higher summit vorticity for two flows. The vorticity in one cardiac cycle along the artery wall for the two pulsatile flows shown in Fig. 16 (a, b) & 17 (a, b). The peak wall vorticity occurs at the throat location which is larger in the Newtonian case (Figs. 16(a) and Fig. 17(a)) than that of the non-Newtonian case (Figs. 16(b) and Fig. 17(b)) during the maximum flow rate $(t = 0.3 * T)$ in case of simple and equivalent pulsatile flow. The minimum vorticity is found at $t = 0.7$ s (Fig. 16(a) and (b)) and $t = 0.55$ s, (Fig. 17(a) and (b)) respectively for two flows.

3.8. Velocity streamlines distribution and development of recirculation

The flow field is further analyzed for streamlines at various time intervals for both Newtonian (Fig. 18(a) and Fig. 19(a)) and non-Newtonian fluid (Figs. 18(b) and Fig. 19(b)) by means of simple and equivalent pulsatile flows. Fig. 18(a), 19(a) and 18(b), 19(b) signify the streamlines parallelisms of Newtonian and non-Newtonian Carreau model blood for both flows at different time intervals through a cardiac cycle for area blockage of 75%. It is mentionable that there is a stable separation zone of flow is made near the artery

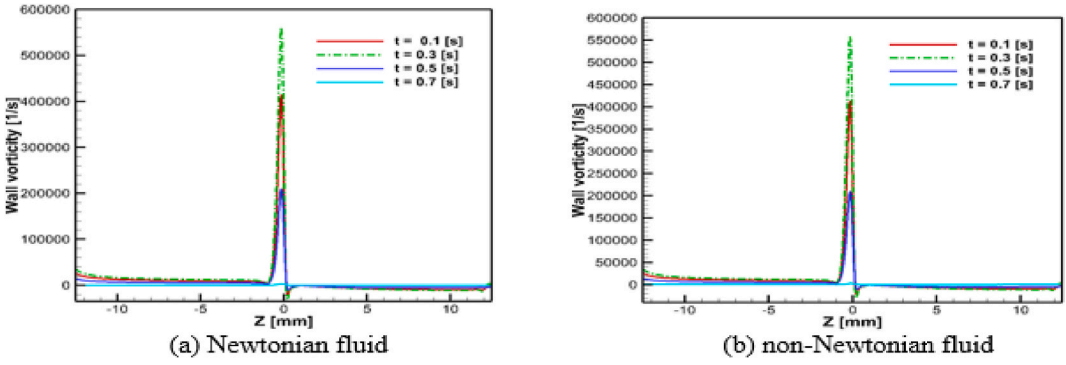

Fig. 16. Vorticity for (a) Newtonian and (b) non-Newtonian fluid along the artery wall for simple pulsatile flow at several time intervals.

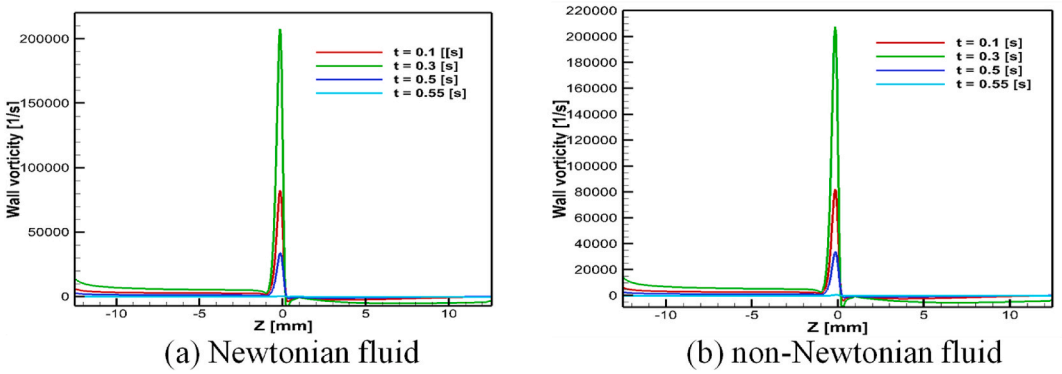

Fig. 17. Vorticity for (a) Newtonian and (b) non-Newtonian fluid along the artery wall for equivalent pulsatile flow at several time intervals.

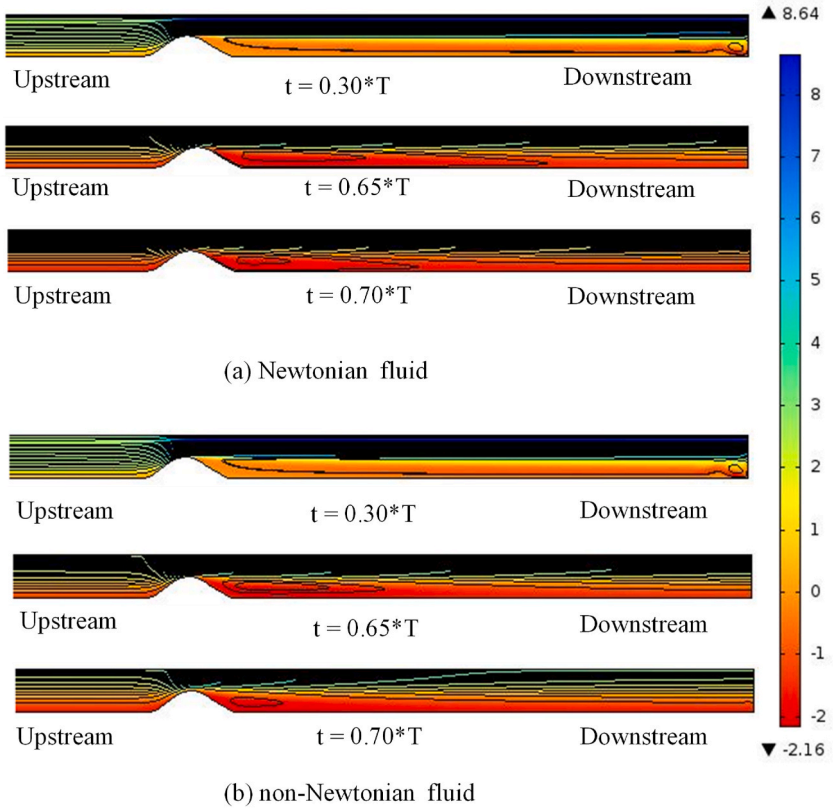

Fig. 18. Streamlines for (a) Newtonian and (b) non-Newtonian fluid at several time intervals for simple pulsatile flow.

wall for most of the pulsatile cycle cases, for both Newtonian and non-Newtonian models, although, its shape and position alter in the pulse cycle. These zones of recirculation are indicative of regions where the reverse flow is formed over a momentous segment of each cycle. Thus, presence of these recirculation zones is of pathological importance as, they increase the time of residence of blood ingredients that may bring about the blood clot or thrombosis. The flow characteristics in simple pulsatile flow (Fig. 18(a) and (b)) for both fluids are almost similar trend because of the identical velocity wave form in the whole cycle except that the Newtonian fluid (Figs. 18(a) and Fig. 19(a)) displays a more disturbed making. The mean flow velocity is lower in the backward half-cycle than the forward one. During the systolic phase $(t = 0.3 * T)$, (Fig. 18(a) and (b)) as the velocity inlet accelerates, the vortex appears downstream of the stenosis throat and becomes larger. It runs to grow even after the decelerates of the flow at $t = 0.5 * T$ (Fig. 18(a) and (b)). The vortex then reduces for $t = 0.65 * T$ (Fig. 18(a) and (b)) and for minimum flow rate $t = 0.7 * T$ (Fig. 18(a) and (b)). After that, when the inflow again arrives at its accelerating phase then the vortex starts to grow and it continues until the end of the artery. Clearly, it is notified that the recirculation length of the non-Newtonian model (Fig. 18(b)) is smaller than that of the Newtonian model

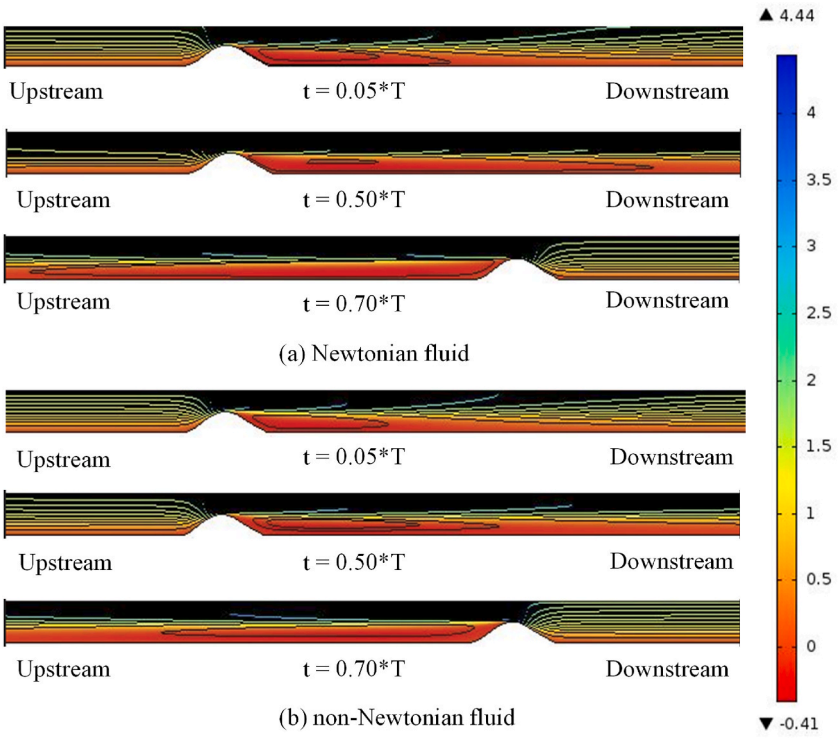

Fig. 19. Streamlines for (a) Newtonian and (b) non-Newtonian fluid at various time intervals for equivalent pulsatile flow.

(Fig. 18(a)) doing.

Furthermore, the flow systems are also observed in the case of equivalent pulsatile flow (Fig. 19(a) and (b)) for Newtonian and non-Newtonian fluids throughout the cardiac cycle and showing until the decelerating phase ($t = 0.5 * T$) (Fig. 19(a) and (b)), the recirculation zone of Newtonian fluid (Fig. 19(a) is larger than the non-Newtonian fluid (Fig. 19(b)) does. During the diastolic phase, the flow reverses direction at the time level $t = 0.70 * T$ (Fig. 19(a) and (b)), and the vortex develops in the pre-stenosis side. Nevertheless, these vortex sizes and their connected separation and reattachment point's positions vary due to Newtonian (Fig. 19(a)) and non-Newtonian fluid (Fig. 19(b)). The Newtonian model provides the greatest separation length, and the non-Newtonian model shows the lowest size separation and a little disturbed pattern flow than its counterpart.

3.9. Hemodynamics recirculation length

The study also focuses on investigating the WSS behaviors at the post-stenosis location. WSS distributions in the post-stenotic zone are shown in Fig. 20 (a, b, c, d) & Fig. 22 (a, b, c, d) (75% AS) for both flows. Since the flow alters significantly during the phases, so the WSS distributions at four several acceleration and deceleration instants ($t = 0.20$ s, 0.30 s, 0.65 s, 0.70 s) (Fig. 20(a), (b), Fig. 20(c) and (d)) and ($t = 0.05$ s, 0.10 s, 0.475 s, 0.50 s) (Fig. 22(a), (b), Fig. 22(c) and (d)) for simple and equivalent pulsatile flows respectively are displayed. The intersection points of WSS curves and the horizontal axis are called the flow separation points at which WSS changes from positive sign to negative sign and are called the reattachment points at which WSS changes from negative sign to positive sign and the length measured from separation to reattachment point is called the recirculation length. Table (2 & 3) indicates the evaluated separation point, reattachment point and recirculation length for different stenosis severity for both inlet profiles, and it is remarkable that the Newtonian fluid predicts the higher recirculation length than the rheological model.

Since the vessel narrows softly due to stenosis, the recirculation lengths of both Newtonian and non-Newtonian fluids increase as exhibited in Figs. 21(b) and 23(b) for $t = 0.3$ s and 0.10 s respectively. The system of the flow fields for more severe stenosis (75%) leads to greater and stiffer vortices in the flow area than the others. For the 30% AS model, WSS is positive at almost time intervals (Table 2 & Table 3) in the post-stenosis zone commencing that there is no flow recirculation at these instants. Figs. 21(a) and 23(a) show the variations of recirculation length in the relatively different times for the 50% AS model. Fig. 20(a), (b), 20(c) & 20(d); Fig. 21 (a) and (b); Fig. 22(a), (b), Fig. 22(c) and (d); Fig. 23(a) and (b) and also Table 2 & Table 3 exhibit the results that the recirculation length of the Newtonian model is greater than that of the Carreau model, and it authenticates the Carreau model prophesy greater viscous dissipation than the Newtonian model. Hence, the application of the Newtonian model related to blood flow investigation should be vigilant for creating more disturbances.

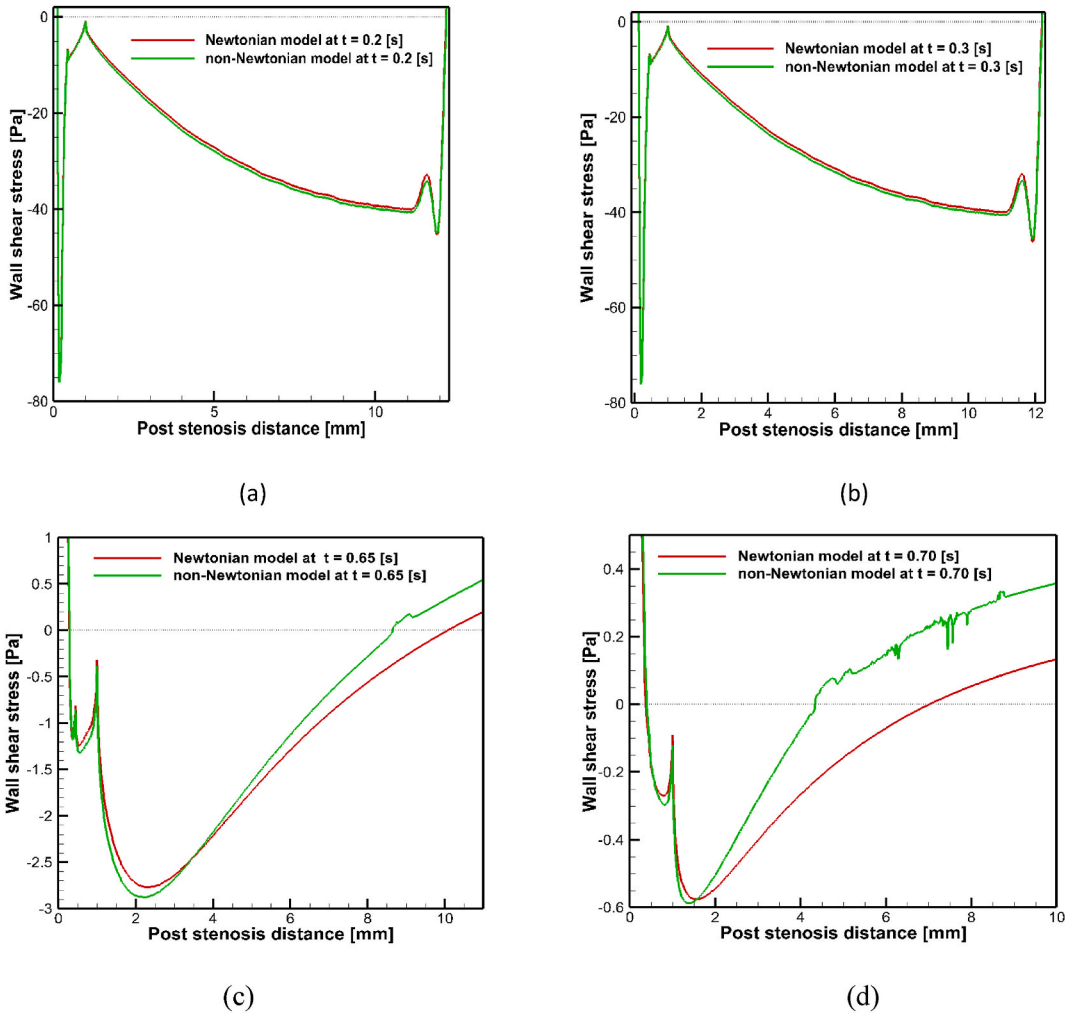

Fig. 20. Shear stress distribution along the post-stenotic wall in the stenosis models at several time levels in the acceleration and deceleration phases of the flow for simple pulsatile inlet velocity.

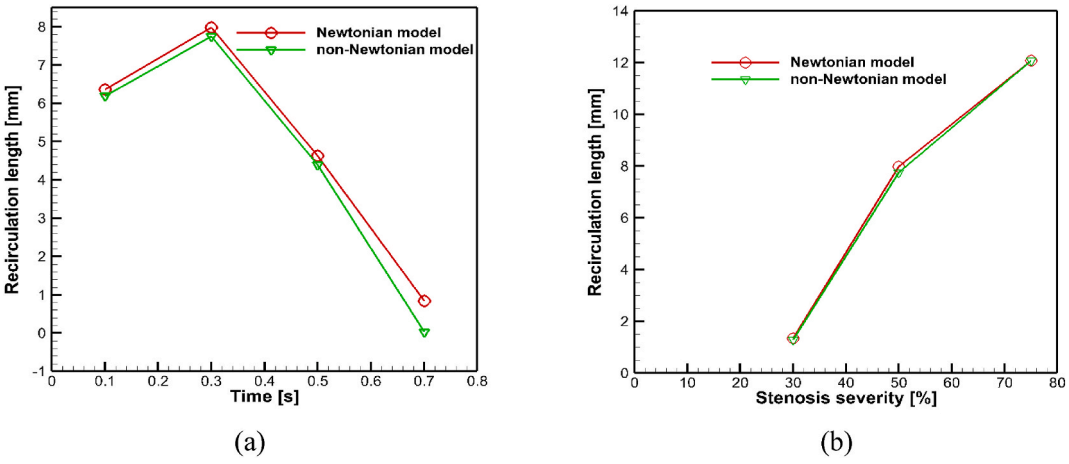

Fig. 21. Recirculation length variations with (a) time of 50% stenosis and (b) stenosis severity at t = 0.3 s for simple pulsatile inlet flow.

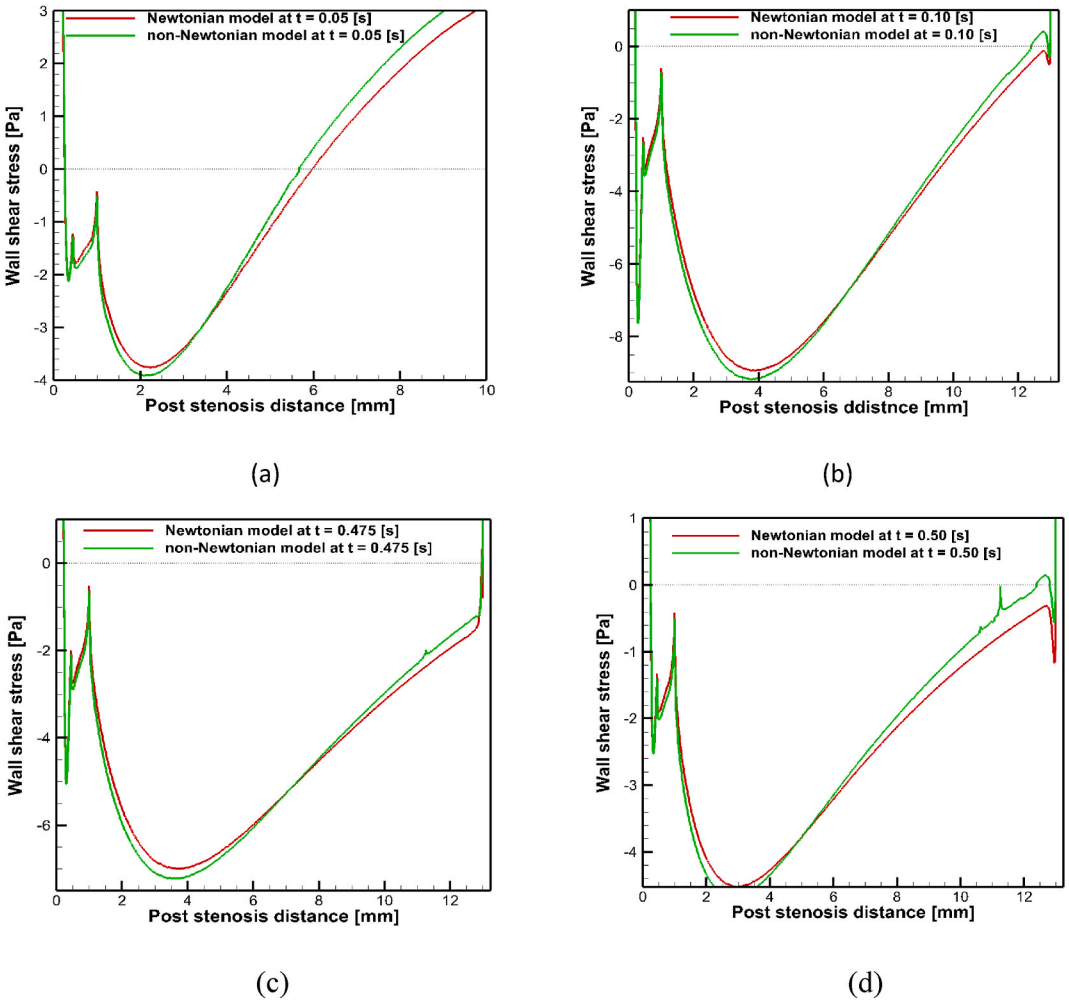

Fig. 22. Shear stress distribution along the post-stenotic wall in the stenosis models at various time levels in the accelerating and decelerating phases of the flow for equivalent pulsatile inlet flow.

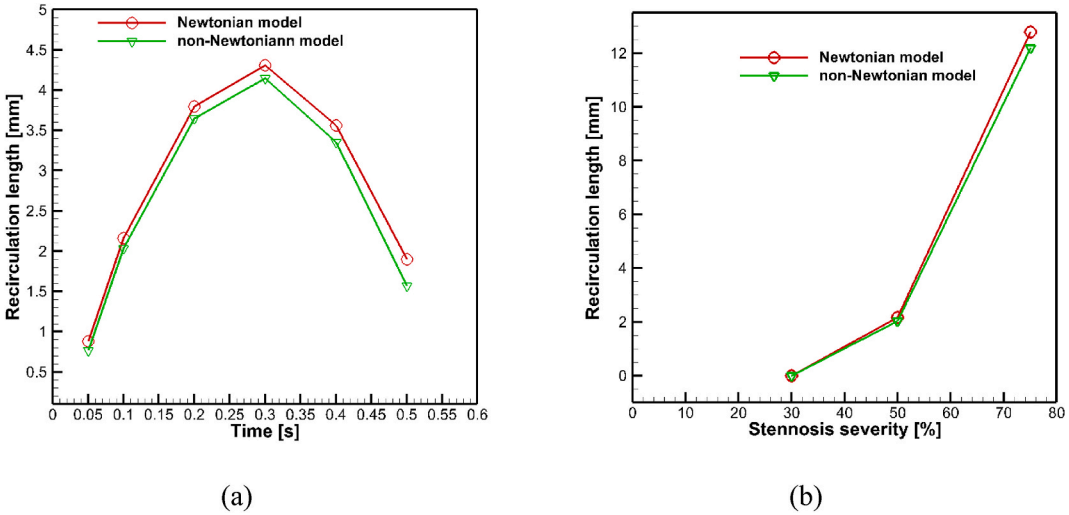

Fig. 23. Recirculation length variations with (a) time of 50% stenosis and (b) stenosis severity at t = 0.1 s for equivalent pulsatile inlet flow.

Table 2
Comparison of separation point, reattachment point and recirculation lengths obtained from Newtonian and non-Newtonian models for simple pulsatile flow.

Model	Time [s]	Phase	AS	Point of separation (PS)	Reattachment point (RA)	Recirculation length [mm]
Newtonian	0.20		30%	0.4882	1.8061	1.3179
	0.30	Accelerating		0.4882	1.8321	1.3439
	0.60	Decelerating		…..	…..	0
	0.65			…..	…..	0
	0.70			…..	…..	0
	0.20	Accelerating	50%	0.2555	8.0856	7.8301
	0.30			0.2555	8.2416	7.9861
	0.60	Decelerating		0.4144	2.6901	2.2757
	0.65			0.5467	1.8060	1.2593
	0.70			0.7296	1.5720	0.8424
	0.20	Accelerating	75%	0.1307	12.2069	12.0762
	0.30			0.1307	12.2070	12.0763
	0.60	Decelerating		0.2168	12.9870	12.7702
	0.65			0.2757	10.0747	9.7990
	0.70			0.3655	7.0195	6.6540
non-Newtonian	0.20	Accelerating	30%	0.4882	1.7801	1.2919
	0.30			0.4882	1.7801	1.2919
	0.60	Decelerating		…..	…..	0
	0.65			…..	…..	0
	0.70			…..	…..	0
	0.20	Accelerating	50%	0.2555	7.8906	7.6351
	0.30			0.2555	8.0076	7.7521
	0.60	Decelerating		0.4263	2.4821	2.0558
	0.65			0.6075	1.5460	0.9385
	0.70			0.9630	0.9877	0.0247
	0.20	Accelerating	75%	0.1307	12.2069	12.0762
	0.30			0.1307	12.2069	12.0762
	0.60	Decelerating		0.2168	12.9868	12.7700
	0.65			0.2757	8.6446	8.3689
	0.70			0.3871	4.3543	3.9672

Table 3
Comparison of separation point, reattachment point and recirculation lengths obtained from Newtonian and non-Newtonian models for equivalent pulsatile flow.

Model	Time [s]	Phase	AS	Point of separation (PS)	Reattachment point (RA)	Recirculation length [mm]
Newtonian	0.05	Accelerating	30%	…..	…..	0
	0.075			…..	…..	0
	0.10			…..	…..	0
	0.475	Decelerating		…..	…..	0
	0.50			…..	…..	0
	0.05	Accelerating	50%	0.5467	1.4290	0.8823
	0.075			0.4263	2.0010	1.5747
	0.10			0.3904	2.5471	2.1567
	0.475	Decelerating		0.4144	2.7031	2.2887
	0.50			0.4500	2.3521	1.9021
	0.05	Accelerating	75%	0.2524	5.9664	5.7140
	0.075			0.2168	9.5027	9.2859
	0.10			0.2047	13.0000	12.7953
	0.475	Decelerating		0.2168	12.9740	12.7572
	0.50			0.2406	13.0000	12.7594
non-Newtonian	0.05	Accelerating	30%	…..	…..	0
	0.075			…. ..	…..	0
	0.10			…..	…..	0
	0.475	Decelerating		…..	…..	0
	0.50			…..	…..	0
	0.05	Accelerating	50%	0.5831	1.3510	0.7679
	0.075			0.4382	1.8840	1.4458
	0.10			0.4024	2.4301	2.0277
	0.475	Decelerating		0.4263	2.4821	2.0558
	0.50			0.4740	2.0400	1.5660
	0.05	Accelerating	75%	0.2524	5.6674	5.4150
	0.075			0.2168	9.1127	8.8959
	0.10			0.2047	12.4019	12.1972
	0.475	Decelerating		0.2168	12.9740	12.7572
	0.50			0.2406	12.4019	12.1613

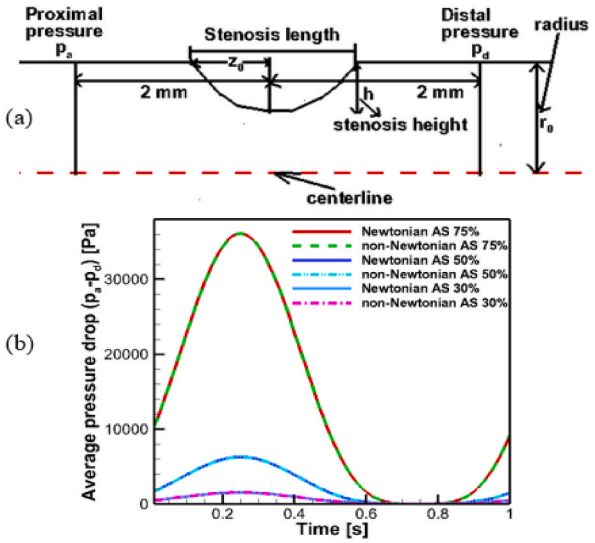

Fig. 24. (a) A schematic diagram and (b) Average pressure drop for Newtonian and non-Newtonian fluids of simple pulsatile flow.

3.10. Average pressure drop for a cardiac cycle

The average pressure drop $(P_a - P_d)$ with respect to time in one cardiac cycle with the various stenosis severity level is ploted in Fig. 24(b). The pressure drop is measured in proximal and distal regions at a distance of 2 mm from the center of the stenosis is shown in the diagram (Fig. 24(a)). Through the Fig. of 24(b) to investigate the top value change, it may be noticed that average pressure drops are lower in the case of 30% and 50% area reductions but a larger appears in the Newtonian model than the non-Newtonian model for simple pulsatile flow in the highest area reduction of 75%.

3.11. Evaluation for treatment on the basis of the diagnostic parameters

Fig. 25(a) shows the impact of several blockage intensities on the pressure drop coefficient (CDP) for both fluids in simple pulsatile inlet flow cases. Concentrating on the impact of blockage intensity on CDP, the grown blockage intensity causes the larger CDP and their relationship approaches to be nonlinear [29]. With greater constriction intensity, the CDP variation turns out more drastic. In accordance with the available literature [10], the value of cut-off is 27.9 for CDP which is exercised by physicians. In the present circumstance, the CDP value is near the critical value for non-Newtonian fluid due to 75% constriction intensity as shown in Fig. 25(a).

As can be observed in Fig. 25(b), the greater blockage intensity increases the LFC value, and their relationship approaches to be linear [29]. In accordance with the literature [11], 0.36 is the critical value for LFC. The LFC value greater than 0.36 suggests the larger

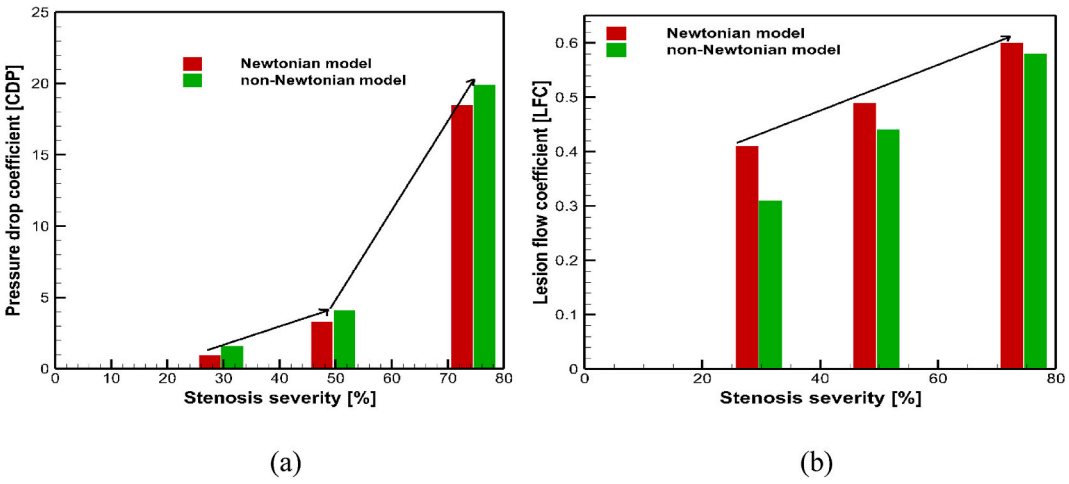

Fig. 25. (a) Coefficient of pressure drop (CDP) and (b) coefficient of lesion flow (LFC) for simple pulsatile flow of Newtonian and non-Newtonian models.

probability of initiated revascularization and ischemia. In the present situation, the LFC value over 0.36 may be obtained up to stenosis intensity of 50% for the non-Newtonian model, and the value of LFC over 0.36 can be acquired when the constriction is up to 30% for the Newtonian model. It can be concluded that the simulated results exceed the critical value, and agreed well with our predicted results of the non-Newtonian fluid [29] than the Newtonian fluid.

B. 3D Bifurcated Left Coronary Artery with LAD and LCx

3.12. 3D methodology validation

The method is also validated with non-Newtonian nature impacts of blood on a pulsatile flow through a bifurcated coronary artery. We have compared the present simulated results with varying angulation of patient specific comparison based idealized coronary artery bifurcation to assure benchmark works. The velocity profiles at the entrance of left circumflex (Fig. 26(a)) and left anterior (Fig. 26(b)) daughter arteries vary according to the bifurcated angulation changes that are well behaved with Rabbi et al. [30] with a maximum error of 4% and minimum error of 0%.

3.13. 3D velocity streamline and velocity contour on a cross-sectional plane

Fig. 27(a and b) presents the velocity magnitude streamlines for peak systole and diastolic phases in one cardiac cycle for Newtonian (Fig. 27(a)) and non-Newtonian fluid (Fig. 27(b)) with a bifurcation angle of 90^0. The velocity streamlines indicate that there are significant separations at the outer wall having reattachment downstream of the bifurcated daughter vessels. It is mandatory to know the flow characteristics between Newtonian and non-Newtonian fluid to detect the effect of hemodynamic parameters on atherosclerotic lesions. Therefore, it is concluded that Newtonian fluid has larger recirculation area as compared to non-Newtonian fluid. As the pulsatile blood flow is transient, the periodic flow variates. Fig. 28 (a, b) displays the velocity contour at three cross-sectional planes at a distance of 5 mm, 10 mm and 15 mm away respectively from the bifurcation point for Newtonian (Fig. 28(a)) and non-Newtonian fluid (Fig. 28(b)) for bifurcation angles of 60^0 and 90^0, sequentially during systolic and diastolic phases. Bifurcation divides the flow into two daughter arteries symmetrically. For the flow recirculation, the curtailed downstream flow is moved towards the inner wall resulting highest velocity is moved to that wall. The magnitude of velocity profiles is decreased with increasing bifurcation angle and a slight difference of velocity magnitude is noticed between Newtonian (Fig. 28(a)) and non-Newtonian fluid (Fig. 28(b)).

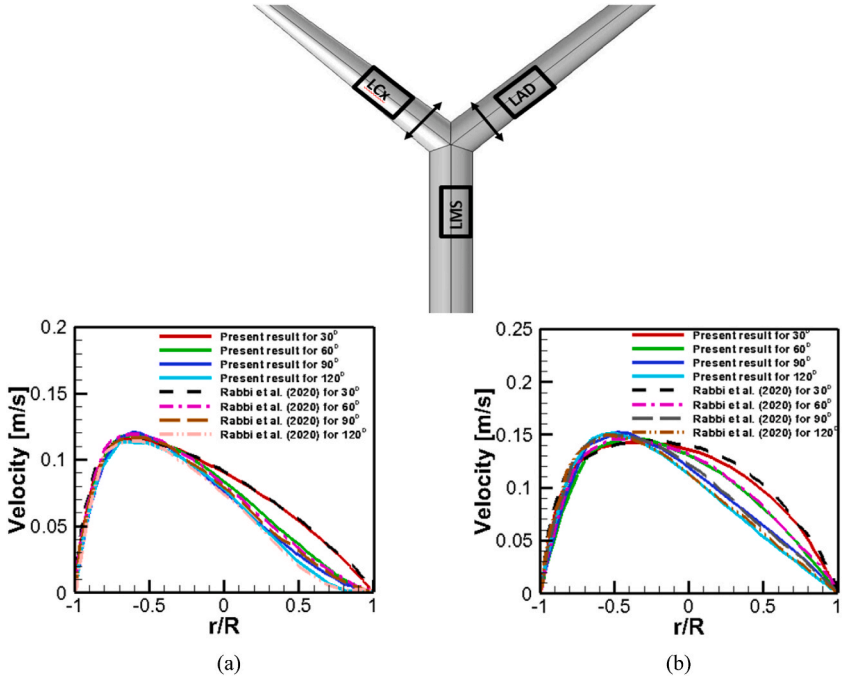

Fig. 26. Velocity profile at (a) left circumflex artery (LCx) and (b) left anterior descending artery (LAD) for $30^0, 60^0, 90^0$ and 120^0 of bifurcation.

3.14. Biomarker indicating TAWSS, OSI and RRT, and time-averaged inlet pressure

Arterial flows can be explained in terms of wall shear stress (WSS) during a complete cardiac cycle, T, near the vessel wall, and the time-averaged wall shear stress (TAWSS), non-dimensional oscillatory shear index (OSI) and relative residence time (RRT) are most familiar indices of wall shear stress. The TAWSS can be calculated as Eq. (11)

$$\mathrm{TAWSS} = \frac{1}{\mathrm{T}} \int_0^{\mathrm{T}} \left| \vec{\tau}_{\mathrm{w}} \right| \mathrm{dt} \tag{11}$$

Where $\vec{\tau}_{\mathrm{w}}$ is the WSS vector, the TAWSS can not state the oscillatory behavior of flows, it gives only average wall shear stress magnitude. Due to oscillatory flow, the research in Ref. [31] proposed the OSI which can be described as Eq. (12)

$$\mathrm{OSI} = \frac{1}{2}\left(1 - \frac{\left| \int_0^{\mathrm{T}} \vec{\tau}_{\mathrm{w}} \mathrm{dt} \right|}{\int_0^{\mathrm{T}} \left| \vec{\tau}_{\mathrm{w}} \right| \mathrm{dt}} \right) \tag{12}$$

Utterly, the relative residence time (RRT) in terms of above stated hemodynamic parameters is introduced in Ref. [32] concerned with blood particles residence time in fluid regions. The RRT can be estimated according to Eq. (13)

$$\mathrm{RRT} = \frac{1}{(1 - 2\mathrm{OSI})\mathrm{TAWSS}} \tag{13}$$

In arterial pulsatile flow, WSS is a biomarker to detect the development and formation of atherosclerosis. The TAWSS contours indicating OSI and RRT for different bifurcated angles are displayed in Fig. 29(A) and (B) due to Newtonian and non-Newtonian fluid. The magnitude of TAWSS normalized by that for Poiseuille wall shear stress due to inlet flow rate in the LMCA for Newtonian viscosity. The maximum TAWSS observe at the top of bifurcation, and that bifurcation generates high velocity gradients by forcing blood near the daughter walls in the area. The outer wall has flow recirculation area by forming thrombus as well as blood clotting with minimum WSS and susceptible to detect the lesions of atherosclerosis and plaque creation. In the inner wall has highly TAWSS over the outer wall (Figs. 29(C) & Fig. 30(b)) with a bifurcation angle of 60° and 90°. TAWSS and bifurcated angle are inversely related, enlightening that with developing angulation, the TAWSS falling and has effect on plaque inclination. The maximum TAWSS outcomes in non-Newtonian fluid (Fig. 30(b)) portray an important indication between Newtonian and non-Newtonian fluid due to the effect of shear-thinning.

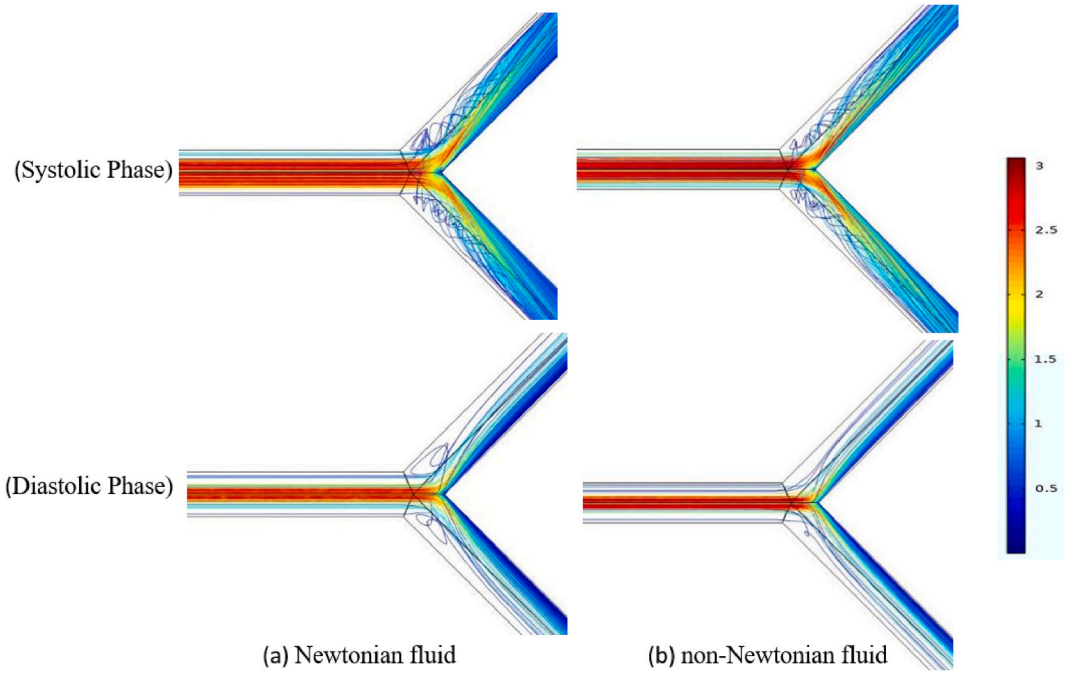

Fig. 27. Streamlines of velocity for fluids of simple pulsatile flow with bifurcation angle of 90^0.

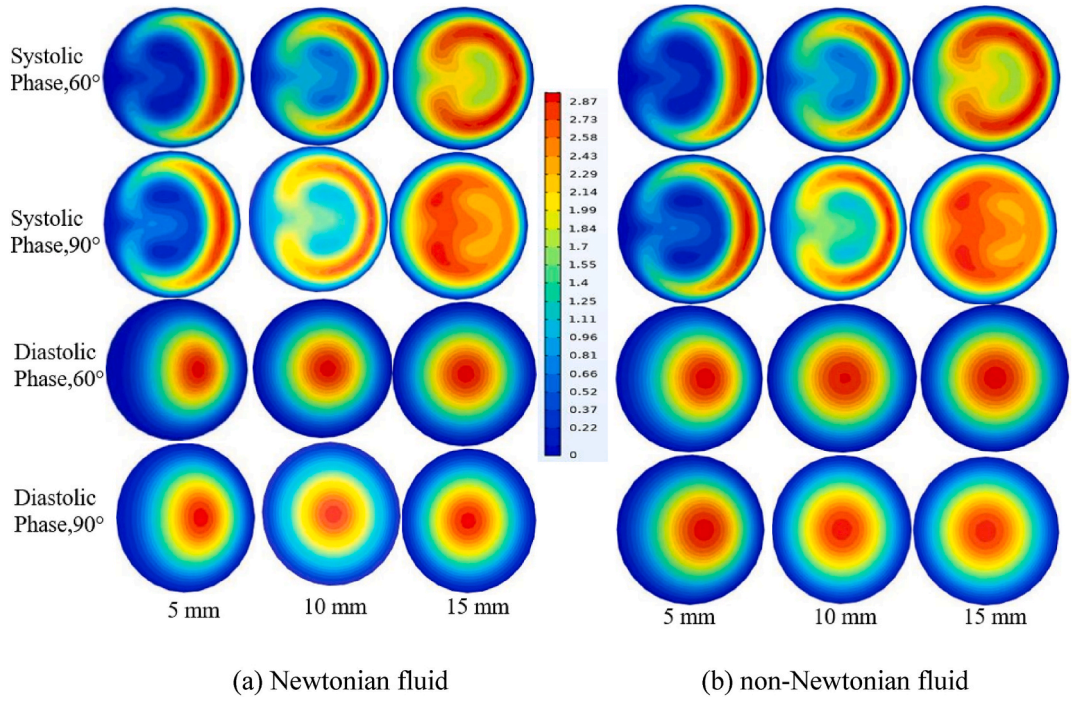

Fig. 28. Velocity magnitude contour on a three cross-sectional plane for (a) Newtonian and (b) non-Newtonian fluid.

Time-averaged inlet pressure for various bifurcation angles due to simple pulsatile flow is presented in Fig. 30 (a). Centerline pressure is the most important predictor for transient blood flow. This study is also based on left coronary artery (LCA) bifurcated models and which indicates an important correlation between bifurcation angle and time-averaged inlet pressure. Results show that the least mean pressure is observed at the centerline for smaller bifurcation angles and mean pressure increases with increasing bifurcation angle. Another important dimensionless hemodynamic parameter OSI is commonly employed to locate the endothelium damaged area throughout the artery of a cardiac cycle. The results show that higher flow separation is noticed at the outer wall due to change the sign of WSS. The maximum OSI is that where the regions of atheroprone initiates and recovers of the vessel. No significant recirculation is concentrated at the inner wall and flow approaches to the downstream resulting OSI is zero. Due to developing the bifurcated angles, the position and shape of flow recirculation zone reduces. The highest bifurcated angles give more oscillating shear stress. RRT is an indicator to locate the area in which particle residence time takes place. At the outer wall OSI and RRT show sequentially in Fig. 30(c) and (d) to represent the atherosclerotic recirculation zone for Newtonian and non-Newtonian fluid and finally concluded that the top point locations of both fluids are not same, and Newtonian fluid has larger reattachment area.

3.15. Non-Newtonian importance factor for simple pulsatile flow

Blood behaves as a non-Newtonian fluid. In an effort to expose a quantitative investigation of the effects of non-Newtonian fluid throughout the left coronary bifurcated artery surface including LAD, LCx within the bifurcated angle, the local importance factor (IFc) estimated as initiated by Johnston et al. [33]. The IFc is identified in Eq. (14)

$$\mathrm{IFc} = \frac{\mu}{\mu_N} \tag{14}$$

where, μ is the effective dynamic viscosity of non-Newtonian fluid and μ_N is the dynamic shear viscosity of Newtonian fluid. Fig. 31 shows the importance factor contour which is related to clinical relevance and is observed for all angulation. The dimensionless value is maximum near bifurcated region (Fig. 31(a, b, c, d)). At the daughter LCx, the cross-sectional importance factor is displayed for systolic and diastolic phases due to all bifurcated angles at a distance of 5 mm from the bifurcation point (Fig. 31(f)). The time-averaged importance factor reduces with increasing bifurcated angulation (Fig. 31(e)). The importance factor is increased at diastolic phases and decreased at systolic phases. This contribution will be implemented for medical treatment as well as cardiovascular diseases.

Analyzing all comparative results, we may summarize the comparison observed using Newtonian & non-Newtonian model as follows:

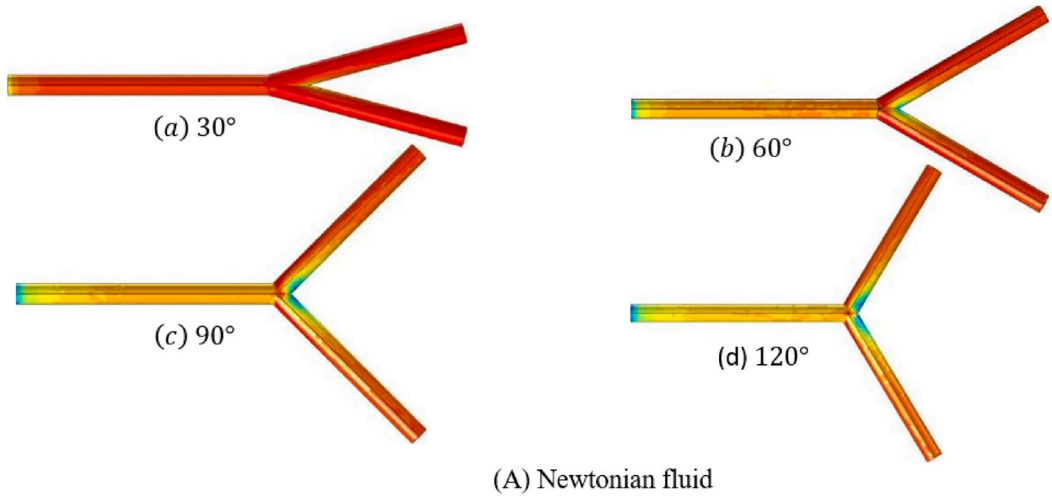

(A) Newtonian fluid

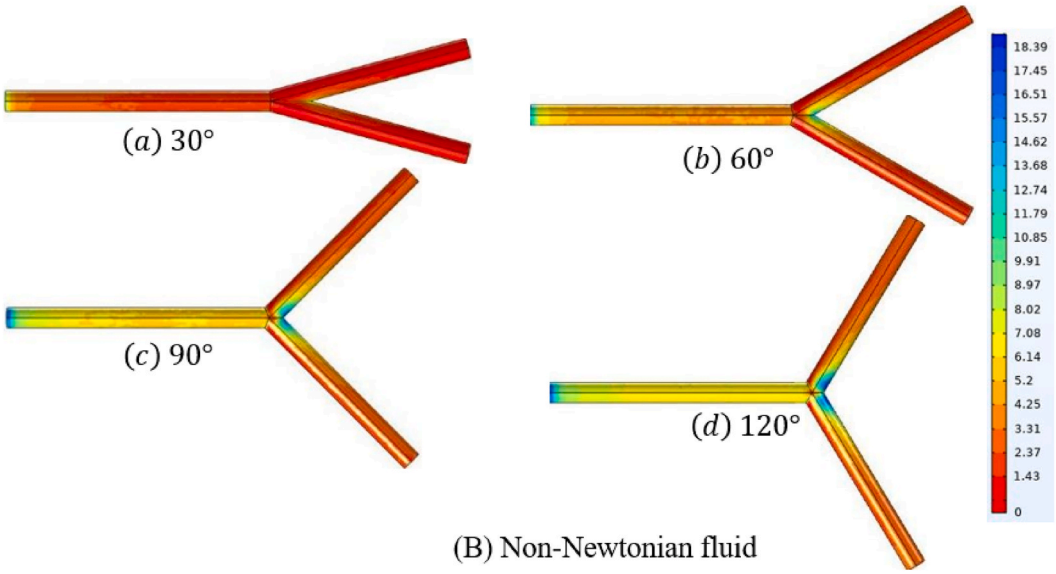

(B) Non-Newtonian fluid

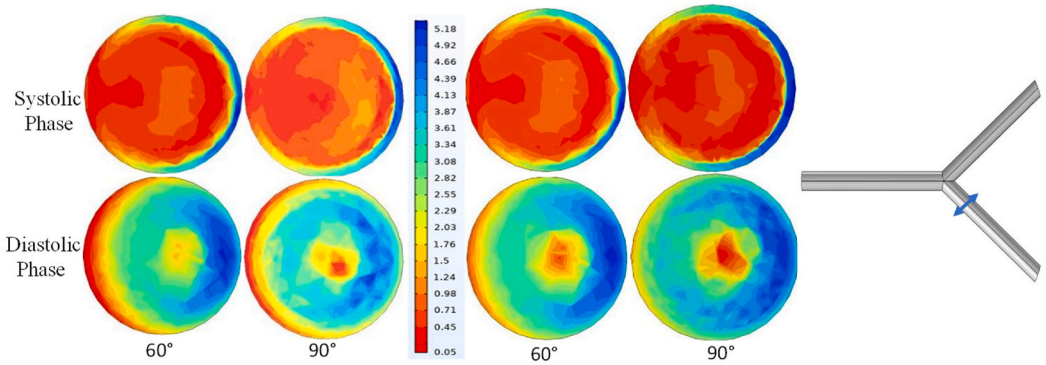

(C)

(caption on next page)

Fig. 29. TAWSS contour for (A) Newtonian, (B) non-Newtonian fluid and (C) cross-sectional shear stress for both fluids of simple pulsatile flow.

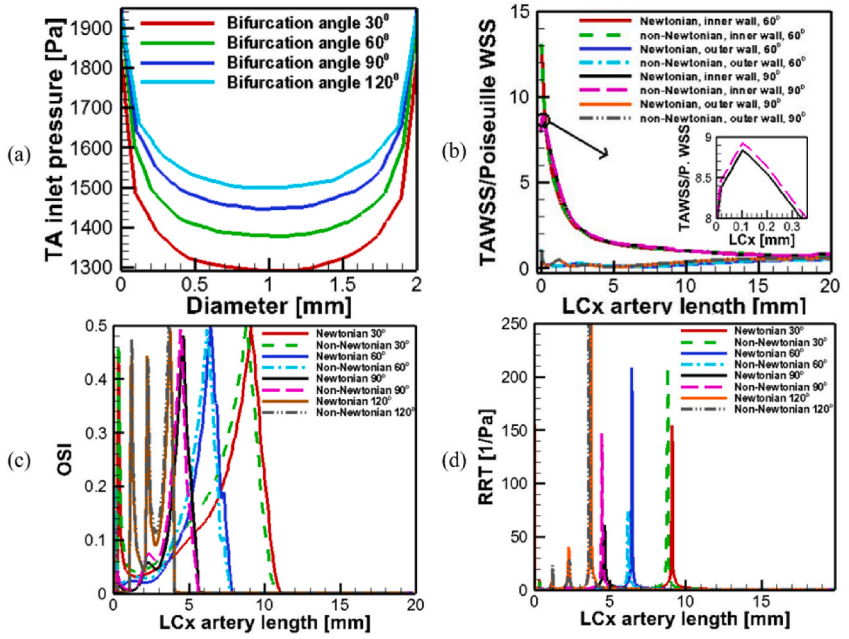

Fig. 30. (a) Time-averaged inlet pressure, (b) TAWSS, (c) OSI and (d) RRT for simple pulsatile flow.

1. The non-Newtonian model provides higher shear stress than that of the Newtonian model for 2D stenotic and 3D bifurcated geometry.
2. The Newtonian fluid exhibits larger recirculation length and wall vorticity in comparison to non-Newtonian fluid for investigated two parts.
3. The CDP and LFC value of the non-Newtonian fluid is near to the critical value of medical assesses for 2D constricted artery.
4. The TAWSS values are higher for non-Newtonian fluid than those of the Newtonian fluid for 3D bifurcated geometry.
5. The location of peak points of OSI and RRT is lower for non-Newtonian fluid than that of the Newtonian fluid in case of 3D bifurcated artery.
6. The simulation time takes longer in the non-Newtonian model.

4. Biomedical implication

On the basis of the approaches of resonance of magnetic as well as ultrasound of intravascular have been discussed to give worthy anatomical and diagnostic actuality, nevertheless, their resolution of spatial as well as temporary is generally not adequate to attain fact based on the distribution of shear stress along the wall in accordance with the velocity gradient in the field of vector. The tactics of computational fluid dynamics (CFD), as opposed to, may contribute an indispensably greater conducive to indication on flow dynamics of coronary artery, with the larger resolution of temporary and spatial, noninvasively, patient specific based and under a totally pragmatic circumstance. The proficiency to carry out patient-specific based simulations of flow in a thoroughly practical surroundings, noninvasively and in this way endlessly, could afford the above-mentioned approaches a momentous act, what one indicates certain computations to be able for predicting potent fulminate situations wherein precautions might be committed. Numerical simulations which can be proposed, evolve the significant supports in this field [29,34–36].

5. Conclusions

The current approach depicts numerical modeling of pulsatile flows through a stenotic and bifurcated artery for hemodynamic behaviors of atherosclerosis. The model is introduced to simulate the blood flow problem for Newtonian and non-Newtonian fluids using two generally employed velocity profiles namely, simple and equivalent pulsatile flows. The numerical model is validated satisfactorily and the predicted outcomes are compared with those available in the literature. The boundary layer thickness is also justified in comparison to the theoretical values. The following outcomes may be summarized on the basis of the findings of this study.

- The Newtonian fluid flow yields a massive separation reign by means of the vortex for 2D and 3D bifurcation geometry to the same inlet velocity.

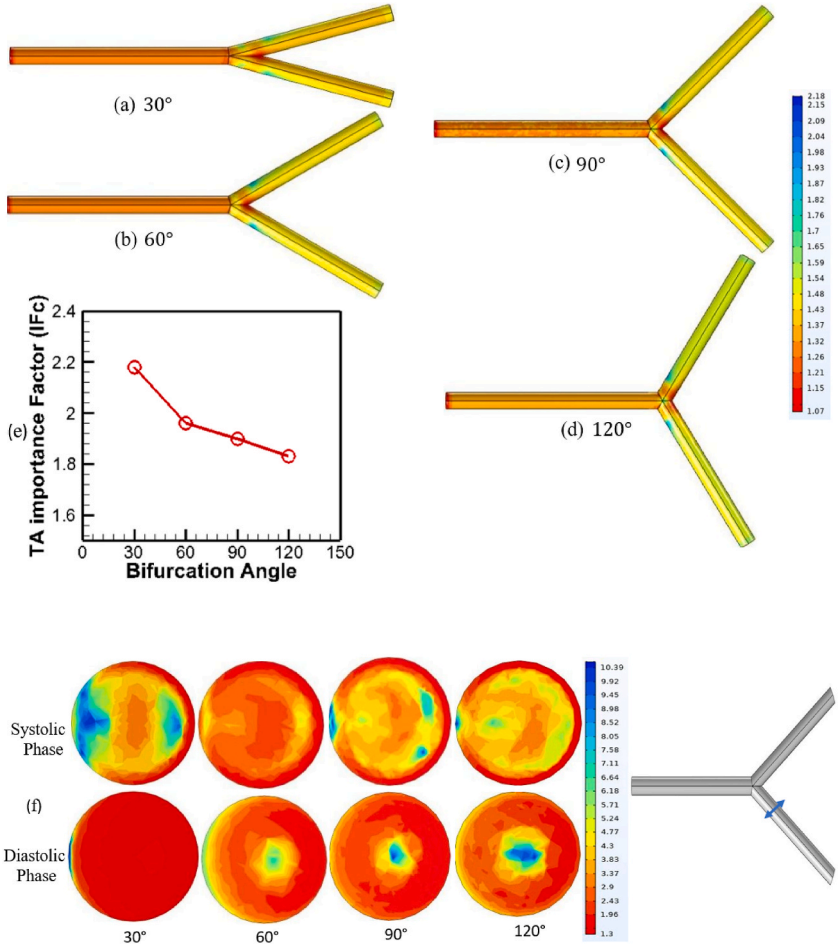

Fig. 31. (a, b, c, d) Time-averaged importance factor (IFc) contour, (e) time-averaged importance factor vs bifurcation angle and (f) importance factor on cross-sectional plane for all angulation.

- The non-Newtonian fluid flow presents greater shear stress at the middle of the constriction for a main stenosed artery.
- Regardless, the rheological model used due to 2D narrowing artery, the nature of shear-thinning blood results in the lower maximum wall vorticity of velocity profiles in comparison to a Newtonian fluid.
- Mostly, the greatest velocity appears at the throat of the blockage as well as the proximal downstream of the constriction for both fluids which is investigated in two-dimensional geometry.
- The pressure falls strongly near the middle of the constriction and recuperates softly since the flow past the constriction for 2D stenotic artery.
- The non-Newtonian fluid provides the better LFC value for 2D stenosed coronary main artery.
- The magnitudes of biomarker indicating TAWSS are higher for non-Newtonian fluid than those of the Newtonian fluid for bifurcated geometry.
- In 3D bifurcation geometry, the TAWSS on the inner wall is higher as compared to that of the outer wall.
- The peak locations of OSI and RRT are not same for Newtonian and non-Newtonian fluids on the branch arteries. High OSI and RRT, and low WSS, are commonly connected with the high possible regions of atheromatous plaque development localization.
- The location of flow reattachment point is reduced for the highest bifurcation angle in bifurcated geometry.
- Time-averaged inlet pressure is minimum for smaller bifurcation angles and the IFc is decreased while the bifurcation angle is increased in 3D bifurcation.

The blockage intensity of the left main coronary artery is deliberated a potential syndrome for revascularization and it is urgent to identify the degree of stenosis associated with the lesion for making a surgical intervention discernment on a patient's atheromatous plaque with a view to avoiding heart attacks or strokes. The diagnostic parameters can be used in the prospective medical practice to provide valuable suggestions to patients for better treatment. Moreover, the effect of bifurcation angles via hemodynamics on the proliferation of atherosclerosis at the regions of bifurcation and the side branch is significant to assess the implications for the clinical treatment.

Author contribution statement

Md. Jashim Uddin, M. Z. I. Bangalee: Conceived and designed the experiments; Performed the experiments; Analyzed and interpreted the data; Contributed reagents, materials, analysis tools or data; Wrote the paper.

M. Ferdows: Performed the experiments; Analyzed and interpreted the data; Contributed reagents, materials, analysis tools or data.

1 - Conceived and designed the experiments;
2 - Performed the experiments;
3 - Analyzed and interpreted the data;
4 - Contributed reagents, materials, analysis tools or data;
5 - Wrote the paper.

Data availability statement

Data will be made available on request.

Declaration of competing interest

The authors declare that they have no known competing financial interests or personal relationships that could have appeared to influence the work reported in this paper.

Acknowledgement

The author would like to acknowledge the funding support from the University Grants Commission (UGC) in Bangladesh. This work was carried out using the computational facilities available in the Department of Applied Mathematics, University of Dhaka, Bangladesh. The Bose Centre for Advanced Study and Research in Natural Sciences, University of Dhaka, Bangladesh also funded partially.

Nomenclature

LMCA	left main coronary artery
2D	two-dimensional
n	index of power law
3D	three-dimensional
OSI	oscillatory shear index
AS	area stenosis
p	pressure
CDP	coefficient of pressure drop
r	radius of artery as a function of z
CFD	computational fluid dynamics
r_0	radius of the unoccluded artery
D	diameter of the artery
r, z	cylindrical co-ordinates
f	frequency
RRT	relative residence time
h	height of the stenosis
t	time
I	identity matrix
T	time period
IFc	importance factor
TA	time-averaged
L	artery length
TAWSS	time-averaged wall shear stress
LAD	left anterior descending artery
$\overline{U}_{d-h}$	time-averaged velocity on the stenosis
LCA	left coronary artery
$\overline{U}_p$	proximal time average velocity
LCx	left circumflex artery
WSS	wall shear stress
LFC	coefficient of lesion flow
z_0	half length of the stenosis

Greek symbols

α	amplitude
μ_∞	viscosity at high shear
$\dot{\gamma}$	rate of shear
π	pi
δ	boundary layer thickness
ρ	density
λ	constant of time
τ	stress tensor
μ	dynamic viscosity
φ	phase angle
μ_0	viscosity at low shear
Δ	difference

References

[1] M.D. Deshpande, D.P. Giddens, R.F. Mabon, Steady laminar flow through modeled vascular stenosis, J. Biomech. 9 (1976) 165–174.
[2] Y. Zhao, H. Wang, W. Chen, W. Sun, X. Yu, C. Sun, G. Hua, Time-resolved simulation of blood flow through left anterior descending coronary artery: effect of varying extent of stenosis on hemodynamics, BMC Cardiovasc. Disord. 23 (2023) 156, https://doi.org/10.1186/s12872-023-03190-2.
[3] K. Tzirakis, Y. Kamarianakis, N. Kontopodis, C.V. loannou, Classification of blood rheological models through an idealized symmetrical bifurcation, Symmetry 15 (3) (2023) 630, https://doi.org/10.3390/sym15030630.
[4] J. Hashemi, B. Patel, Y.S. Chatzizisis, G.S. Kassab, Study of coronary atherosclerosis using blood residence time, Front. Physiol. 12 (2021), 625420, https://doi.org/10.3389/fphys.625420.
[5] S. K. Kadhim, M. G. A. Azawy, S. A. G. Ali, M. Q. Kadhim, The Influence of Non-Newtonian Model on Properties of Blood Flow Through a Left Coronary Artery with Presence of Different Double Stenosis, International Journal of Heat & Technology 39(3) (2021) 895 – 905, https://doi.org/10.18280/ijht.390324.
[6] A.M. Awad, K.S. Mekheimer, S.A. Elkilany, A.Z. Zaher, Leveraging elasticity of blood stenosis to detect the role of a non-Newtonian flow midst an arterial tube: mazumdar and Keller models, Chin. J. Phys. 77 (2022) 2520–2540.
[7] K.S. Mekheimer, I. Shahzadi, S. Nadeem, A.M.A. Moawad, A.Z. Zaher, Reactivity of bifurcation angle and electroosmosis flow for hemodynamic flow through aortic bifurcation and stenotic wall with heat transfer, Physica Scripta 96 (1) (2021), 015216.
[8] S.Y. Motlagh, S. Deyhim, Numerical study of magnetic drug targeting inside the bifurcated channel as a simplified model of right common iliac artery using Fe304-blood magnetic nanofluid, Iranian J. Sci. Tech. Transact. Mech. Eng. 47 (1) (2023) 51–65, https://doi.org/10.1007/s40997-022-00507-y.
[9] F. He, X. Wang, L. Hua, T. Guo, Non-Newtonian effects of blood flow on hemodynamics in pulmonary stenosis: numerical simulation, Appl. Bionics Biomech. 2023 (2023), 1434832, https://doi.org/10.1155/2023/1434832.
[10] K.K. Kolli, I. Arif, S.V. Peelukhana, P. Succop, L.H. Back, T.A. Helmy, M.A. Leesar, M.A. Effat, R.K. Banerjee, Diagnostic performance of pressure drop coefficient in relation to fractional flow reserve and coronary flow reserve, J. Invasive Cardiol. 26 (2014) 2–9.
[11] S.V. Peelukhana, R.K. Banerjee, T.P. van de Hoef, K.K. Kolli, M. Effat, T. Helmy, M. Leesar, H. Kerr, J.J. Piek, P. Succop, L. Back, I. Arif, Evaluation of lesion flow coefficient for the detection of coronary artery disease in patient groups from two academic medical centers, Cardiovasc. Revascularization Med. 19 (3) (2018) 348–354.
[12] L.C. Cheng, M.E. Clark, J.M. Robertson, Numerical calculations of oscillating flow in the vicinity of square wall obstacles in plane conduits, J. Biomech. 5 (1972) 467–484.
[13] W. Liao, T. S Lee, H.T. Low, Numerical studies of physiological pulsatile flow through constricted tube, Int. J. Numer. Methods Heat Fluid Flow 14 (2004) 689–713.
[14] P. Halder, A. Husain, M. Zunaid, A. Samad, Newtonian and Non-Newtonian pulsatile flows through an artery with stenosis, J. Eng. Res. 14 (2017) 191–205.
[15] A. Razavi, E. Shirani, M.R. Sadeghi, Numerical simulation of blood pulsatile flow in a stenosed carotid artery using different rheological models, J. Biomech. 44 (2011) 2021–2030.
[16] P. Youssefi, et al., Impact of patient-specific inflow velocity profile on hemodynamics of the thoracic aorta, J. Biomech. Eng. 140 (2018) 1–14.
[17] M. Mahmoudi, A. Farghadan, D. McConnell, A.J. Barker, J.J. Wentzel, M.J. Budoff, A. Arzani, The story of wall shear stress in coronary artery atherosclerosis: biochemical transport and mechanotransduction, J. Biomech. Eng. 143 (2021), 041002.
[18] M. Nagargoje, R. Gupta, Effect of asymmetry on the flow behavior in an idealized arterial bifurcation, Comput. Methods Biomech. Biomed. Eng. 23 (6) (2020) 232–247.
[19] E. Lakzian, P. Akbarzadeh, Numerical investigation of unsteady pulsatile Newtonian/non-Newtonian blood flow through curved stenosed arteries, Bio Med. Mater. Eng. 30 (2019) 525–540.
[20] Z. Abbas, M.S. Shabbir, N. Ali, Numerical study of magnetohydrodynamic pulsatile flow of sutterby fluid through an inclined overlapping arterial stenosis in the presence of periodic body acceleration, Results Phys. 9 (2018) 753–762.
[21] COMSOL Multiphysics, Reference Manual, Version 5.2.
[22] A. Otero-Cacho, A.P. Munuzuri, The geometry of coronary artery bifurcations and its role in plaque formation, Clinical Cardiol. Cardiovascular Med. 4 (1) (2022) 24–30.
[23] K. Jozwik, D. Obidowski, Geometrical models of vertebral arteries and numerical simulations of the blood flow through them, in: Proceedings of the 3rd Frontiers in Biomedical Devices Conference and Exhibition, 2008, pp. 75–79. June 18-20.
[24] S. Ahsaas, S. Tiwari, Numerical simulation of blood flow through asymmetric and symmetric occlusion in carotid artery, in: Proceedings of the 3rd International Conference on Fluid Flow, Heat and Mass Transfer, 2016, pp. 170–178.
[25] F.J.H. Gijsen, F.N. van de Vosse, J.D. Janssen, The influence of the non-Newtonian properties of blood on the flow in large arteries: steady flow in a carotid bifurcation model, J. Biomech. 32 (1999) 601–608.
[26] G.R. Zendehbudi, M.S. Moayeri, Comparison of physiological and simple pulsatile flows through stenosed arteries, J. Biomech. 32 (1999) 959–965.
[27] Nagargoje, et al., Pulsatile flow dynamics in symmetric and asymmetric bifurcating vessels, Phys. Fluids 33 (2021) 1–22.
[28] R.K. Banerjee, et al., Concurrent assessment of epicardial coronary artery stenosis and microvascular dysfunction using diagnostic endpoints derived from fundamental fluid dynamics principles, J. Invasive Cardiol. 21 (10) (2009) 511–517.
[29] J. Song, S. Kouidri, F. Bakir, Numerical study of hemodynamic and diagnostic parameters affected by stenosis in bifurcated artery, Comput. Methods Biomech. Biomed. Eng. 23 (2020) 1–12.

[30] M.F. Rabbi, F.S. Laboni, M.T. Arafat, Computational analysis of the coronary artery hemodynamics with different anatomical variations, Inform. Med. Unlocked 19 (2020) (2020), 100314.
[31] X. He, D.N. Ku, Pulsatile flow in the human left coronary artery bifurcation: average conditions, J. Biomech. Eng. 118 (1996) 74–82.
[32] H.A. Himburg, D.M. Grzybowski, A.L. Hazel, J.A. LaMack, X.M. Li, M.H. Friedman, Spatial comparison between wall shear stress measures and porcine arterial endothelial permeability, Am. J. Physiol. Heart Circ. Physiol. 286 (2004) H1916–H1922.
[33] B.M. Johnston, P.R. Johnston, S. Corney, D. Kilpatrick, Non-Newtonian blood flow in human right coronary arteries: steady state simulations, J. Biomech. 37 (5) (2004) 709–720.
[34] C.L. Feldman, P.H. Stone, Intravascular hemodynamic factors responsible for progression of coronary atherosclerosis and development of vulnerable plaque, Curr. Opin. Cardiol. 15 (6) (2000) 430–440.
[35] R. Krams, J.J. Wentzel, J.A.F. Oomen, et al., Evaluation of endothelial shear stress and 3D geometry as factors determining the development of atherosclerosis and remodeling in human coronary arteries in vivo: combining 3D reconstruction from angiography and IVUS (ANGUS) with computational fluid dynamics, Arterioscler. Thromb. Vasc. Biol. 17 (10) (1997) 2061–2065.
[36] P.H. Stone, A.U. Coskun, S. Kinlay, et al., Effect of endothelial shear stress on the progression of coronary artery disease, vascular remodeling, and in-stent restenosis in humans: in vivo 6-month follow-up study, Circulation 108 (4) (2003) 438–444.